Student thesis series INES nr 266

Integration of LiDAR data and satellite imagery for biomass estimation in conifer-dominated forest

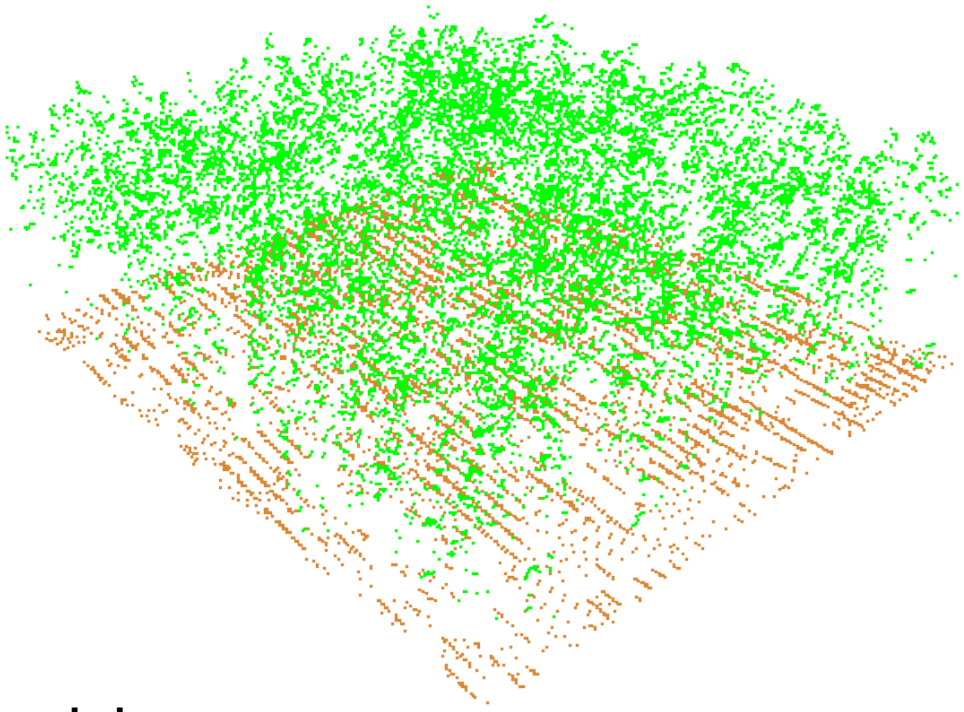

Iurii Shendryk

2013
Department of
Physical Geography and Ecosystem Science
Lund University
Sölvegatan 12
S-223 62 Lund
Sweden

Iurii Shendryk (2013). Integration of LiDAR data and satellite imagery for biomass estimation in conifer-dominated forest

Master degree thesis, 30 credits in Physical Geography and Ecosystem Analysis
Department of Physical Geography and Ecosystem Science, Lund University

Cover image:
3D subset of LiDAR point cloud used in this study (visualization in Mars Explorer software)

Integration of LiDAR data and satellite imagery for biomass estimation in conifer-dominated forest

---

Iurii Shendryk

Master degree thesis in Physical Geography and Ecosystem Analysis, 30 credits

Supervisor:
Dr. Margareta Hellström
Department of Physical Geography and Ecosystems Science
Lund University

Department of Physical Geography and Ecosystems Science,
Lund University, Sweden, 2013

Abstract

As a first step in the assessment of carbon flux between the terrestrial environment and the atmosphere it is important to accurately quantify the carbon stock of forest ecosystems. LiDAR technology, in this respect, has proved to be a valuable tool, able to provide accurate estimates of aboveground biomass (AGB). The overall goal of this study was to develop a simplified method for assessing AGB for individual trees using remote sensing in conifer-dominated forest in the southwest of Sweden. Vegetation classification of SPOT-5 image has been done in order to improve AGB estimates based on biomass dependence on vegetation types. Both local maximum algorithm using a constant size evaluation window and inverse watershed segmentation methods were used for forest inventory parameter extraction from a LiDAR-derived canopy height model. Final estimation of AGB was conducted using regression models derived from measured tree parameters in the field. Field measurements were performed over 83 plots by recording trees' species, height and diameter at breast height (1.3 m). Results showed AGB to vary from less than 1 kg/m^2 in very young forests up to 94 kg/m^2 in mature spruce forests with *RMSE* of 2 kg/m^2 and 4.7 kg/m^2, respectively. Linear regression models showed that the introduction of the watershed segmentation does not improve the results (R^2 = 0.79) in comparison to the results derived from local maximum algorithm using a constant size evaluation window (R^2 = 0.83). Availability of AGB estimates allows further studies of carbon stocks as well as monitoring of this forest ecosystem for disturbance and change.

Key words: LiDAR, SPOT-5, remote sensing, aboveground biomass (AGB), vegetation classification, digital elevation model (DEM), canopy height model (CHM), tree segmentation

Sammanfattning

Ett första steg i arbetet att uppskatta kolflödet mellan landbaserade ekosystem och atmosfären är att så precist som möjligt analysera kvantiteten ovanjordisk biomassa. LiDAR teknologi har i detta avseende visat sig vara ett värdefullt verktyg. Det överlöpande målet med denna studie är att utveckla en förenklad metod, baserad på fjärranalys, för att uppskatta ovanjordisk biomassa för individuella träd över barrträdsdominerad skog i sydvästra Sverige. Eftersom mängden biomassa är beroende av vegetationstyp, har en vegetationsklassificering utförts i studieområdet. Både en lokal maximeringsalgoritm, som använder ett konstant utvärderingsfönster, och en så-kallad invers avrinningsområdessegmentationsmetod användes för extraktion av skogsinventerings-parametrar från en LiDAR-data baserad trädkronhöjdmodell. Den slutliga uppskattningen av ovanjordisk biomassa gjordes utifrån regressionsmodeller framtagna utifrån trädparametrar mätta i fält. Fältmätningarna gjordes för 83 jordlotter, där trädart, höjd och diameter (vid brösthöjd, 1.3 m) mättes. Resultaten visar att ovanjordisk biomassa varierar mellan mindre än 1 kg/m^2 för väldigt ung skog up till 94 kg/m^2 för mogen barrskog med ett standardfel (*RMSE*) på 2 kg/m^2 och 4.7 kg/m^2, respektive. Linjära regressionsmodeller visade att användningen av avrinningsområdessegmentering inte förbättrar resultaten (R^2 = 0.79) i jämförelse med resultat från en lokal maximeringsalgoritm baserad på ett konstant utvärderingsfönster (R^2 = 0.83).

Nyckelord: LiDAR, SPOT-5, fjärranalys, ovanjordisk biomassa, vegetationsklassificering, digital höjdmodell , trädkronhöjdmodell, trädsegmentering

Popularized summary

Globally, carbon dioxide (CO_2) is of great concern, as it is partly responsible for the increasing greenhouse effect, causing global warming. It is hypothesized that conifer-dominated forest in Västra Götaland County may be a large source of greenhouse gases (GHG) including CO_2. Forest biomass stores a lot of carbon, which is exchanged in the form of CO_2 with atmosphere through respiration and photosynthesis in the process known as carbon cycle. In order to approve or reject the hypothesis it is important to quantify the fluxes of CO_2 from this drained, highly fertile coniferous forest. As a first step for achieving this task the amount of carbon stored in the forest should be estimated. Therefore, the overall goal of this study is to develop a simplified method for assessing aboveground biomass (AGB) for individual trees using remote sensing. In this study, AGB represents the sum of stem, bark, branch and foliage biomasses. The developed model was based on the use of airborne laser scanning and an image from the SPOT-5 satellite. The capability of laser systems to directly provide height measurements allowed us to derive the tree height of individual trees, while SPOT-5 image allowed us to classify tree types of the studied area. These two inputs were used for calculating AGB over the whole area of study and compared against AGB measured in the field based on parameters such as trees' species, height and diameter. The overall accuracy of the developed model, when comparing AGB estimates from remote sensing with field observations was equal to 80 %, which proved the validity of the methodology applied. Availability of AGB estimates allows further monitoring of this forest ecosystem for disturbance or change. Furthermore, AGB values can be directly used in further studies of carbon stocks in the area.

Key words: LiDAR, SPOT-5, remote sensing, aboveground biomass (AGB), vegetation classification, digital elevation model (DEM), canopy height model (CHM), tree segmentation

Table of contents:

List of figures:

List of tables:

List of abbreviations:

AGB – Aboveground Biomass

CHM – Canopy Height Model

CR – Crown Biomass

DBH – Diameter at Breast Height

DEM – Digital Elevation Model

DN – Digital Number

DSM – Digital Surface Model

DTM – Digital Terrain Model

GHG – Greenhouse Gas

GPS – Global Positioning System

IWS – Inverse Watershed Segmentation

LAGGE – Landscape Greenhouse Gas Exchange

LiDAR – Light Detection and Ranging

MIR – Middle Infrared Reflectance

NASA – National Aeronautics and Space Administration

NIR – Near Infrared Reflectance

PAEK – Polynomial Approximation with Exponential Kernel

RGB – Red Green Blue

RMSE – Root Mean Square Error

SSE – Sum of Squares due to Error

SSR – Sum of Squares of the Regression

SST – Total Sum of Squares

ST – Stem Biomass

TIN – Triangulated Irregular Network

Acknowledgements

First of all I want to express my gratitude to Dr. Margareta Hellström at the Department of Physical Geography and Ecosystems Science, who has introduced me to the LAGGE project and its objectives. As a supervisor of my thesis she has always been very supportive by sharing her knowledge and experience with me.

A special thank you goes to Prof. Leif Klemedtsson from Gothenburg University, for his scientific input as coordinator of LAGGE project and Elin Julén from the same university, who provided direct assistance during my fieldwork. I also want to thank Dr. Ivan Tishaev from Taras Shevchenko National University of Kyiv for giving initial suggestions on how to perform this research, and Samuel Cook at the University of Cambridge for help with proofreading.

Finally, I am thankful to the people at Lund University, the Technical University of Denmark and Stockholm University who have helped me with everything from discussing the use of statistical methods to actual processing of geospatial data.

This study was financially supported by Landscape Greenhouse Gas Exchange (LAGGE) project and therefore I wish to express my sincere gratitude to the people in charge of this project. Additional funding was also provided by the master studies program of the Department of Physical Geography and Ecosystem Science, Lund University.

1. Introduction

This master thesis was conducted in the frame of the Swedish inter-university research cooperation project called Landscape Greenhouse Gas Exchange (LAGGE). One of the main goals of the LAGGE project is to quantify the net fluxes of greenhouse gases (GHG) from a drained, highly fertile coniferous forest as it is considered to be a large net source of GHG. Globally, the GHG of greatest concern is CO_2 *(IPCC, 2007)* and an understanding of the carbon cycle may be considered as one of the fundamental steps in addressing issues related to global warming. As a preliminary step in assessment of the carbon flux between the terrestrial environment and the atmosphere it is important to accurately quantify the carbon stock of forest ecosystems. The carbon stock of forests is a basic parameter for understanding carbon exchange between the atmosphere and the forest ecosystem and represents an amount of carbon contained in a 'pool', such as aboveground forest biomass (AGB) *(Houghton, 2005).* Therefore, the overall goal of this study was to develop a simplified method for assessing AGB for individual trees using remote sensing. It will be investigated how elevation information, such as discrete-return LiDAR data from airborne systems used together with spectral information from satellite imagery, may allow robust estimates of AGB in conifer-dominated forest in southwest Sweden.

The hypotheses addressed in this study were:

1) Multispectral SPOT-5 data can be used to provide an accurate forest mapping on species level.
2) Discrete-return LIDAR data may be used to estimate AGB through the use of allometric relationships to levels that are not significantly different from field measured AGB values.

In relation to the second hypothesis the priority task was to check the feasibility of using a relatively low point density LiDAR dataset in conjunction with satellite imagery for individual tree level AGB estimation.

1.1. Background

Biomass and carbon stock assessment of forest ecosystems gained importance in connection with the Climate Convention and the Kyoto Protocol *(IPCC, 2007).* In this context, biomass presents a huge interest, as it determines the magnitude and rate of autotrophic respiration as well as the amount of carbon emitted to the atmosphere when the ecosystem is disturbed *(Houghton et al, 2009).* Therefore, estimation of the biomass stored in forests may be considered as a key area of research for understanding the global carbon cycle *(Lefsky et al, 2001).*

The forest carbon cycle involves carbon exchange between the atmosphere, soil and biomass, whose carbon stock change should be estimated. However, it is still a challenging task to give an accurate estimate of the forest biomass. So far, our understanding of terrestrial biomass amounts and distribution has been primarily based on ground measurements of limited areas

with many regions remaining unmeasured *(Houghton et al, 2009).* At the same time, direct estimation of AGB via ground surveys is both time-consuming and expensive and generally repeated only at ten-year intervals *(Houghton, 2005).* Therefore, the possibility of biomass estimation using remote sensing is considered to be a good alternative or complement to conventional ground-based methods *(Hese et al, 2005).*

A substantial number of previous studies have shown that different remote sensing techniques can be used for AGB estimation. Both passive remote sensing techniques as well as active have been applied in order to explore their potential in biomass studies. Estimation of forest carbon stock is difficult for optical and radar sensors, though it was successful in some cases on a forest stand level. For example, *Mette et al (2004)* used polarimetric synthetic aperture radar interferometry for forest biomass extraction through forest height-biomass allometry. According to their study, both the height extraction and the allometric biomass conversion performed well over dense forest stands. However, it is widely recognized that LiDAR represents the future of biomass estimation on a single tree level, and, as such, has become widely used in vegetation studies *(Evans et al, 2009; Jochem et al, 2011).*

LiDAR (Light Detection and Ranging) is an active remote sensing system which transmits pulses of laser light toward the ground by means of a scanning mirror. The time between sent and reflected pulses is measured and converted into a distance measurement, which is used for derivation of a 3D elevation surface *(Popescu, 2007; Lewis and Hancock, 2007).* A pulse generated by a LiDAR system is in the near infrared or visible part of the electromagnetic spectrum (900 – 1064 nm) and can penetrate the vegetation canopy during data acquisition *(Evans et al, 2009).*

The capability of LiDAR systems to provide height measurements allows us to derive the vertical extent of forest stands. Using this capability, various methodologies have been developed for extracting biomass using both discrete-return and full waveform LiDAR systems *(Lefsky et al, 2001; Bortolot and Wynne, 2005; Popescu, 2007; Edson and Wing, 2011).* Discrete-return LiDAR systems have a small footprint (typically 20 – 80 cm in diameter) and are able to record one to several returns through the forest canopy depending on the laser energy intensity returned to the sensor. In contrast, waveform sensors have larger footprints (10 – 100 m) and digitize the complete waveform of each returned pulse in fixed distance intervals *(Evans et al, 2009; Lewis and Hancock, 2007).*

One of the main considerations when assessing AGB using discrete-return LiDAR data is the point density of measurements. Generally, AGB estimation at individual tree level requires high point densities of more than 5 points/m^2 and is based on regression models using LiDAR-derived parameters, such as tree height, and estimates of AGB measured in the field *(Jochem et al, 2011).* In this way, *Popescu (2007)* developed a method for biomass extraction from LiDAR-derived tree height and crown diameter in combination with regression models at individual tree level. For individual tree extraction he used a window of variable size over the canopy height model (CHM) in order to locate local maximum. Variable window size implies that for low trees smaller window was used than for tall trees. In his study the model performance for AGB estimation at individual tree level was good with R^2 of 0.93, thus

proving the usefulness of airborne LiDAR data for forest inventory parameters extraction *(Popescu, 2007).*

A comparison of commonly-used algorithms for individual tree parameter derivation and subsequent estimation of biomass was undertaken by *Edson and Wing (2011)* for mixed and spruce forest sites. Three software algorithms to delineate and measure the forest including FUSION, TreeVaW *(Popescu, 2007),* and inverse watershed segmentation *(Andersen, 2009)* were tested. By using the output form mentioned above (tree delineation software algorithms), the biomass was estimated and compared to biomass estimates from the field. The results demonstrated that biomass predicted by FUSION and TreeVaW was underestimated by 25 % and 31 % respectively, while watershed segmentation produced overestimation of about 10 %. It was also noted that using the FUSION algorithm, which analyzes LiDAR point clouds, was favorable compared to TreeVaW and watershed segmentation, which both rely only on a canopy height model (CHM) for extraction of forest inventory parameters. The main drawback of methods using CHM is the inability to use points from trees existing under primary canopy, which are eliminated in rendering the CHM surface *(Edson and Wing, 2011).*

Although, there were many successful attempts to estimate AGB using LiDAR data, it is still considered to be a challenging task in terms of model complexity and data availability. Furthermore, the research in the area of LiDAR data integration with vegetation classes derived from satellite imagery for estimation of AGB is not well documented. Therefore, this study, among other things, is going to address the possibility of integrating LiDAR-derived tree heights with vegetation types derived from satellite imagery. According to *Chen et al (2012)* the integration of optical imagery and LiDAR data can result in substantial improvement of biomass estimates compared to the use of LiDAR data alone.

1.2. Study area

The Skogaryd study area (58°22′10″ N, 12°08′47″ E) is located in southwest Sweden (Västra Götaland county) and occupies an area of approximately 30.5 km^2 (Figure 1). The topography of this region is characterized by an average elevation above sea level of 80 m, with a minimum of 50 m and a maximum of 110 m and predominately gentle slopes. The main soil types are highly organic postglacial clays and silts.

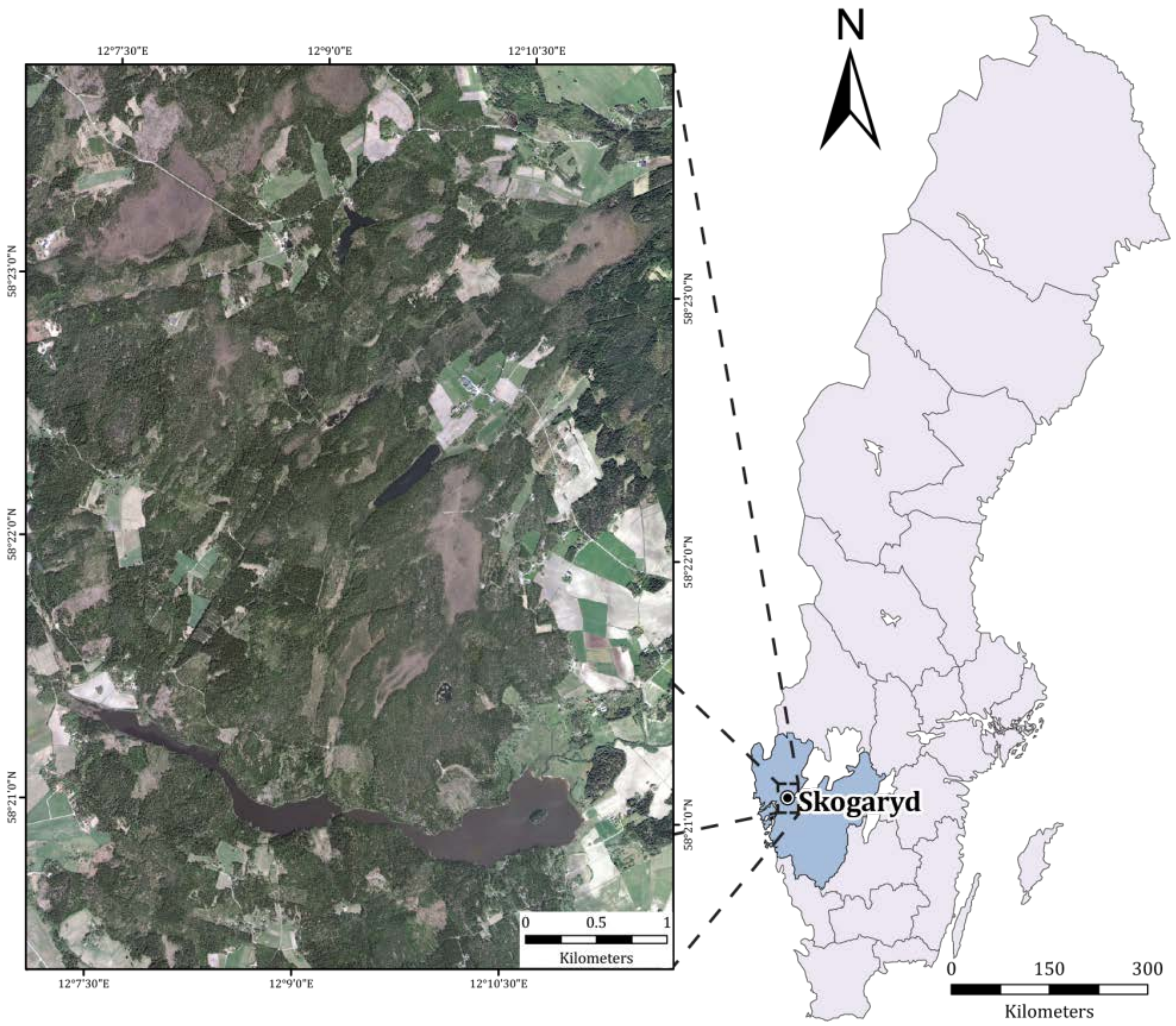

Figure 1. Map of Sweden with location of the study area being zoomed to RGB orthophoto image on the left. Source: *@ Lantmäteriet, Dnr: i2012/927.*

The forest in the Skogaryd area is highly fertile and has drained soils covered by stands of spruce, pine and birch in various developmental stages and is owned by private citizens. Figure 2 illustrates typical types of forest encountered during fieldwork. In most cases forest stands were dominated by coniferous species with rare occurrence of deciduous or mixed species. Variations in mineral composition of the soil and management practices across the Skogaryd area resulted in different densities and stages of forest maturity. The typical representatives of flora beneath the canopy layer consisted of species such as juniper and blueberry. The ground layer was often covered by feather moss with a certain amount of fallen trees on it.

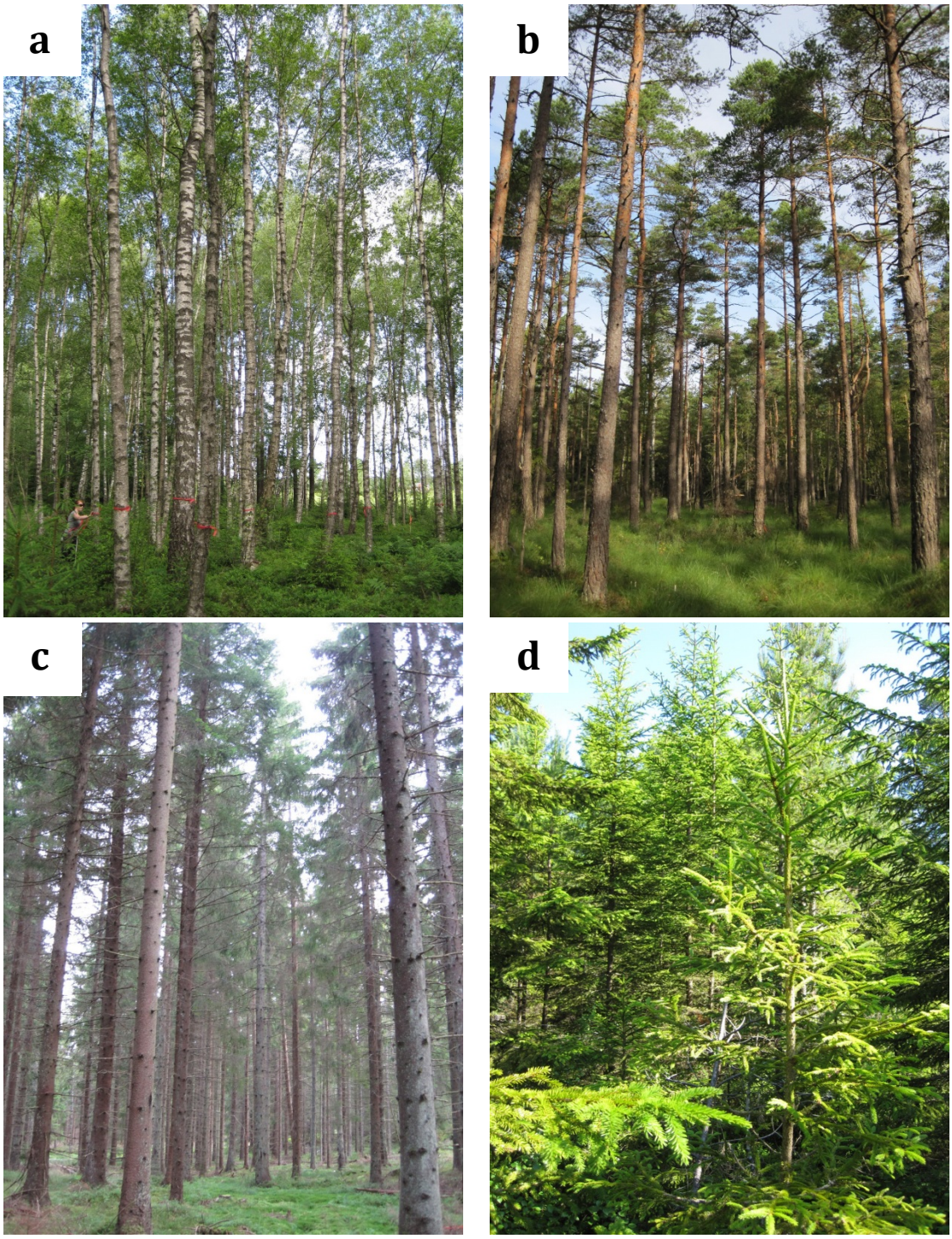

Figure 2. Typical types of forest encountered during fieldwork in the Skogaryd: a) Plot #6: deciduous mature forest b) Plot #69: pine mature forest c) Plot #47: spruce mature forest, d) Plot #11: spruce young forest *(photos taken during fieldwork).* Spatial location of plots may be viewed in Appendix 2.

Overall, the area is characterized by a patchy landscape with dominant coniferous forests. However, lakes and bogs as well as agricultural fields are scattered throughout the region and such a fragmented landscape has historically been formed due to farming and rural development.

2. Materials and Methods

To manage, visualize, process and analyze airborne LiDAR data and optical imagery, two commercial software packages were used: ESRI ArcGIS 10.1 and Merrick & Company MARS Explorer 7.0. In addition, SAGA GIS software was used for individual tree segmentation using inverse watershed algorithm and MathWorks MATLAB 2012b for statistical analysis. The methodology used for AGB estimation was mainly based on integration of approaches from previous studies.

2.1. Measured field data

The fieldwork in the Skogaryd was performed for the purpose of collecting ground truth data and was divided into two phases. The first phase ran from June 26th to July 6th, 2012. The second phase was performed from August 21st to August 27th, 2012. Trees within a total of 83 square field plots of approximately 15 m by 15 m were measured for diameter at breast height (DBH). The tree height measurements were performed only in 18 of the surveyed plots, mainly due to time constraints and difficulties associated with treetop detection in highly dense forest stands. These tree parameters represent the most important element of this project, as they were required for AGB estimation. The delimitation of plots in the field was done using ordinary measuring tape and was often complicated in highly dense forest. The coordinates of the plot centers were measured using a 'Magellan Explorist 510' GPS unit with preinstalled topographic maps of the area studied and maximum accuracy of 4 m. The coordinates were collected with GPS in geographic coordinates (lon/lat) on the WGS 1984 ellipsoid and later transferred in GIS format and reprojected in the SWEREF99 coordinate system. The location of the 83 plots measured in the field is presented in Appendix 2 for assessment of the sampling scheme. Figure 3 shows the equipment used during fieldwork for individual tree parameter measurements. The tree diameter measurements were performed with calipers, while tree heights were measured using a highly accurate hypsometer (Vertex IV) with a height resolution of 0.1 m. The Vertex IV is an instrument designed for precision height and distance measurement using ultrasonic signals *(Haglöf, 2012)*. In order to measure the tree height, the accompanying transponder was fastened to the tree at breast height (approx. 1.3 m). Then the user moved away from the tree to a distance approximately equal to the tree height and recorded up to three height readings for the treetop. Figure 4 demonstrates this procedure.

Figure 3. Fieldwork equipment: calipers, GPS unit, hypsometer, transponder, measuring tape, measuring stick and field log *(photo taken during fieldwork)*.

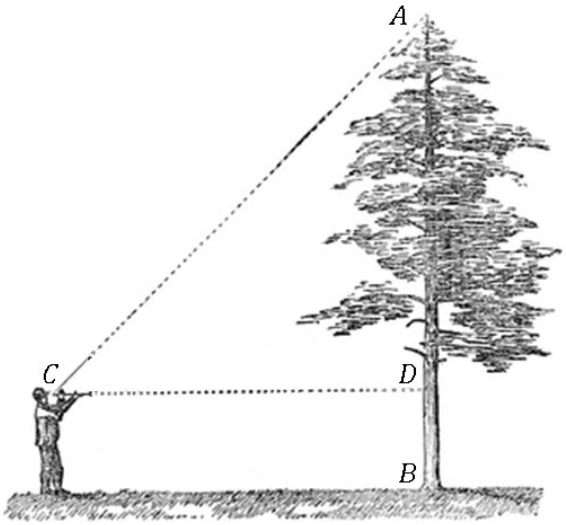

Figure 4. Tree height measurements procedure. *A* – tree top, *B* – ground surface, *C* – user's position, *D* – transponder's position (*Haglöf, 2012).*

During both phases of fieldwork an additional 230 ground control points were collected for validation of the vegetation classification.

2.2. Remotely sensed data

All remotely sensed data available for this project were provided by the Swedish Land Survey *(@ Lantmäteriet, Dnr: i2012/927)* as part of a collaboration with Swedish universities including Lund University. Remotely sensed imagery consisted of orthorectified SPOT-5 images with 10 m spatial resolution and four spectral bands (green, red, near-infrared and mid-infrared) acquired on July 29th, 2011 and aerial orthophoto with 1 m spatial resolution from 2009. These types of data were primarily used for vegetation classification. In addition, a discrete return airborne LiDAR dataset, obtained on July 3rd, 2011 using the Leica ALS50-II airborne LiDAR system was used as the basis for canopy height determination.

LiDAR data covered the whole area of interest (approx. 30.5 km^2) and consisted of point clouds with multiple returns (up to 5). The point density varied from less than 0.0625 to 1 points/m^2 with an average density of 0.8 points/m^2 and can be viewed in Appendix 3. The varying point density of the LiDAR data is mainly a consequence of overlapping flight strips *(Jochem et al, 2011)*. The scanner had a footprint size of around 0.5 m and a scanning angle of ± 20 º. The mean flight altitude was 2000 m. The x, y, z data was georeferenced to the SWEREF99 coordinate system and the RH2000 height system. Points were preclassified by Swedish Land Survey into three classes: unclassified, ground and water using automated routines in TerraScan software *(Lantmäteriet, 2012)*.

2.3. Vegetation classification

Initially, a preliminary vegetation classification was performed as a basis for the fieldwork planning. Afterwards, the data collected in the field served as an input to final classification. In both instances similar methodologies were applied. Classification of vegetation species was

exclusively based on the orthorectified SPOT-5 image, which was initially georeferenced by Swedish Land Survey. Georeferencing took into account the Earth's curvature, height differences, parallax errors and others factors that displace the image data *(Lantmäteriet, 2012).* A precision of less than 0.1 pixels was achieved.

2.3.1. Feature isolation

In order for any other cover type not to interfere with the classifier of forest pixels, it was important to delineate accurate and up-to-date boundaries of forest stands. The extraction of forest stands for preliminary classification was based on a relatively coarse and outdated land cover map, which was developed by the Swedish Land Survey in 2007 due to the unavailability of LiDAR data at the beginning of this project. After obtaining access to a LiDAR dataset of the study area it was possible to derive an accurate vegetation mask, which has potentially improved final classification. This was achieved by vectorization of a digital terrain model (DTM) *(see chapter 2.4.2)* and its subsequent refining by excluding all forest vegetated and unvegetated areas with a total area less than 1000 m^2. The resulting vector mask was smoothed using the PAEK (Polynomial Approximation with Exponential Kernel) method and used for clipping out orthorectified SPOT-5 image.

2.3.2. Classification scheme

An important issue in remote sensing vegetation mapping is to select a suitable classification scheme *(Muise, 2011).* Considering that remote sensing can only detect optical signatures of different species, the following classes were developed: pine, spruce and deciduous forest. As coniferous forest was of special interest for this study, both spruce and pine classes were additionally divided into different age classes. A threshold of 15 cm in diameter at breast height was used for determination of tree maturity. Such a division will allow for example the monitoring of young forest stands only, which is important for growth projections *(Edson and Wing, 2011).*

2.3.3. Supervised Maximum Likelihood Classification

By analyzing data collected in the field and spectral information (orthophoto) available from the study site, training areas for final vegetation classification were selected. Forest sites surveyed in the field with species homogeneity of more than 80 % were considered when choosing training areas. When working with orthophoto images, it was difficult to identify subtle differences between vegetation types. Applying a stretch renderer such as histogram-equalization made it easier to pick out areas of different vegetation species. The recommended number of pixels per training area is 10 to 100 times the number of bands in the imagery. Generally such a number of pixels will supply the classifier with sufficient information to classify each pixel in the image *(Muise, 2011).* Thus, training areas of around 200 pixels per class were created for further classification analysis. A final scheme with training areas statistics used for classification of the SPOT-5 image in this study is shown in Table 1.

Table 1. Classification scheme and training areas statistics.

Species:	DBH threshold (cm)	Homogeneity ratio (%)	Sample size (pixels)
Spruce mature	≥ 15	> 80	212
Spruce young	< 15	> 80	216
Pine mature	≥ 15	> 80	210
Pine young	< 15	> 80	158
Deciduous	2 - 40	> 80	210

One of the traditional supervised classification algorithms, the Maximum Likelihood algorithm, was selected. It calculates the probability of the information class membership for each pixel based on the probability density function. Each pixel is assigned to the information class with the highest probability *(Mehner et al, 2004).* The resulting classified image was smoothed using the 3 by 3 majority filter in order to get rid of noise in the form of single misclassified pixels.

2.4. LiDAR analysis

An important challenge when estimating AGB was the ability to accurately extract individual trees and their canopy height from the discrete-return airborne LiDAR dataset. This was achieved by using a simple algorithm to classify potential canopy returns and their following segmentation into individual trees. The effectiveness of the algorithm applied was verified using the measured data in the field.

2.4.1 Point cloud classification

The raw LiDAR data were provided by the Swedish Land Survey as a point cloud classified into three classes: ground, water and unclassified. Three additional classes: high vegetation, buildings and reserved were created by applying automated algorithms in MARS Explorer software. High vegetation class was defined as all points in the range 2 m to 40 m as calculated from triangular irregular network (TIN) ground surface using a 'height from ground' algorithm. This range of heights was chosen based on the lowest (2 m) and highest (35 m) trees measured in the field. All points having a height value of less than 2 m remained unclassified and potentially represented points reflected from very young trees, bushes or stones. Buildings were classified using a 'building' filter, which identifies relatively smooth surfaces built from the points in the seeding classifications point set *(Merrick & Company, 2012).* The seeding classifications point set contained points strongly identified as canopy. In addition, by knowing exact coordinates of all artificial high-rise structures, such as eddy-covariance towers, it was easy to classify these points manually into the reserved class. This was done in order to exclude erroneously classified vegetation points from digital surface model (DSM) calculation. An example of the final classification of LiDAR points cloud can be found in Figures 5 and 6.

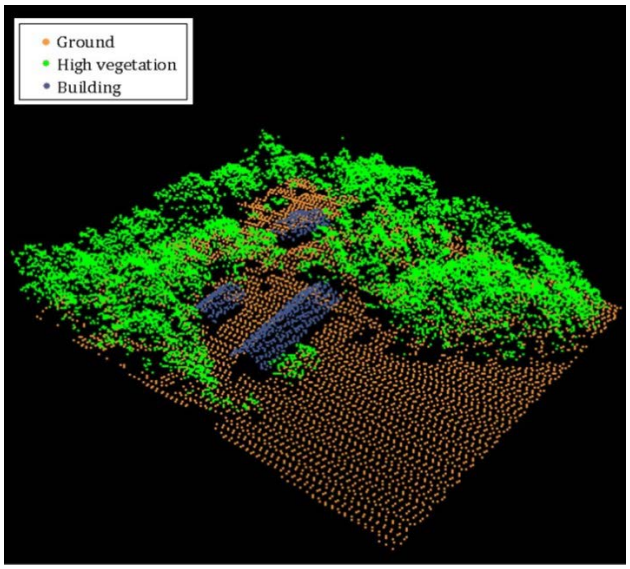

Figure 5. 3D subset of classified LiDAR points over the Skogaryd area. Area is approximately 40 m by 40 m.

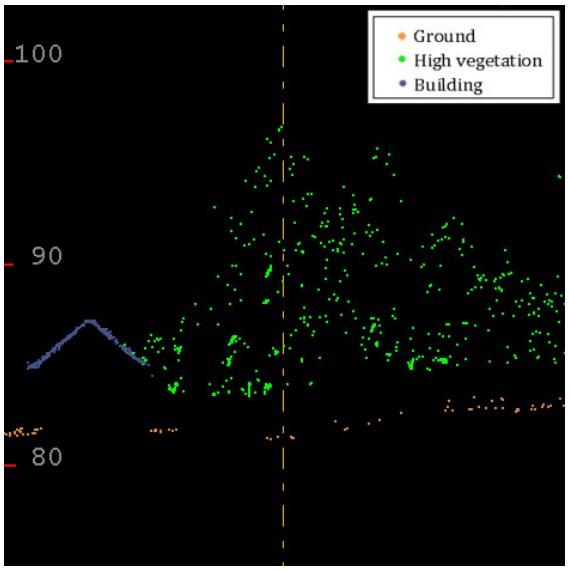

Figure 6. 2D subset of classified LiDAR points over the Skogaryd area. Profile is 2 m wide.

It is also important to note that the absence of major power lines over the area of study facilitated the classification scheme.

2.4.2. Digital elevation models extraction

A digital elevation model (DEM) represents height information without any specifications as to the surface and is used as a generic term for digital surface model (DSM) and digital terrain model (DTM) *(Peckham, 2007)*. A DTM, which represents the bare ground surface without any objects like plants and buildings, was derived by building a geodatabase of terrain from all points in the ground class and converting it to a raster format with a cell size of 3 m (Appendix 4). A rule of thumb used when deciding on a cell size for DTM was to set it at four times the average point spacing *(ESRI, 2011)*. A DSM, which represents the earth's surface and includes all objects on it, was built using only the first returns in the high vegetation class. Other returns were considered to be not representative of canopy height but rather provided information on canopy structure *(Edson and Wing, 2011)*. When creating the DSM, only LiDAR points with maximum elevation in 0.5 m by 0.5 m cells were used. This cell size was chosen based on average point density to allow an accurate delineation of the canopy surface *(Popescu, 2007)*. Gap filling of the resulting DSM was performed using a 3 by 3 mean filter. Finally, a canopy height model (CHM) was derived by simple subtraction of the DTM height value from the DSM height value in each pixel. The CHM may be described as a 3D surface that contains information about vegetation heights above ground surface *(Popescu, 2007)*. A 3D example of a CHM over a small area of the study is presented in Figure 7, while a complete map of the CHM can be viewed in Appendix 5.

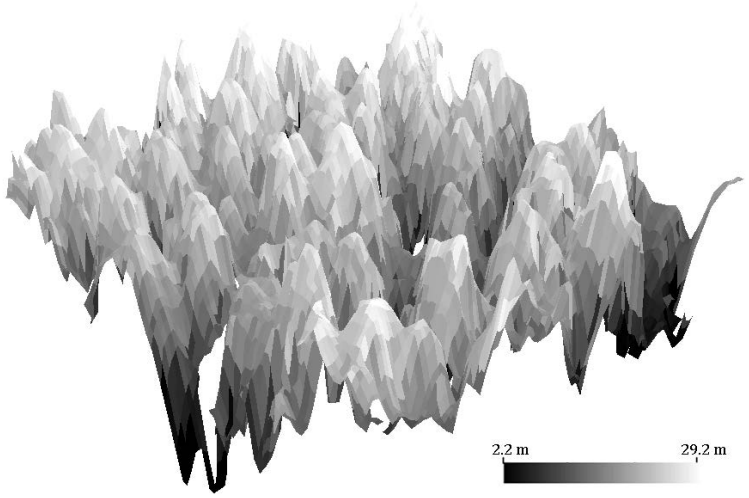

Figure 7. The subset of canopy height model derived from LiDAR data over the Skogaryd.

Initially, the LiDAR data was checked for the presence of any inconsistencies or anomalies. The overlap, of at least 200 meters, between scanned areas resulted in quite inconstant spacing between points with an average point density of 0.8 points/m^2 and a range between 0.1 and 1 points/m^2 *(Lantmäteriet, 2012)*. Consequently, lower accuracies are expected when extracting digital elevation models (DEM) in areas with relatively low point densities.

2.4.3. Individual tree segmentation

It is widely accepted that extraction of individual trees from the CHM may improve the estimates of AGB as it allows canopies to be treated as independent entities *(Bortolot and Wynne, 2005).* In this study, an approach for individual tree delineation was applied in the form of local maximum algorithm using a constant size evaluation window. The method implies the extraction of maximum values from the CHM by using a search window of user-defined size. This introduces direct underestimation or overestimation of AGB depending on the window size used. Window sizes of 2 m by 2 m and 3 m by 3 m were tested in order to examine the impact of changing cell sizes on biomass estimation. Both these methods were constrained in terms of tree canopy delineation and were not able to detect more than 56 and 25 trees per plot, respectively. The better approach would be to use local maximum algorithm with variable-size window, where window size is directly proportional to the tree canopy height. Such an algorithm is implemented in FUSION and TreeVaW software as described in *Edson and Wing (2011)*. Unfortunately, this approach was not properly tested due to time and resources constraints.

Another method for individual tree canopy delineation used in this study was an inverse watershed segmentation (IWS) algorithm. IWS is one of the methods commonly used for extraction of forest inventory parameters at an individual tree level from a LiDAR-derived CHM *(Edson and Wing, 2011).* When applied, the inverted canopy surface raster is segmented into the equivalent of individual hydrologic drainage basins by identification of local maximum and the nearest minima values *(Andersen, 2009)*. Thus, IWS is potentially able to delineate distinct tree entities with height values and raster crown diameter from the CHM. In this project, this algorithm was applied using freeware SAGA GIS software. It was

assumed that IWS would improve the accuracy of biomass estimations in comparison to a local maximum approach with a constant window.

2.5. Statistical accuracy assessment

The final step in analyzing and interpreting remote sensing data is statistical accuracy assessment, which provides important information about the quality of the maps and the usefulness of the model developed *(Congalton, 1991).*

2.5.1. Vegetation classification

Statistical accuracy assessment in the context of vegetation classification is required in order to make a more objective evaluation than can be achieved visually. An independent sample of ground validation points located across the investigation area with a random spatial distribution pattern was used for a statistical accuracy assessment of vegetation classification. Initially 230 collected ground truth points were refined by excluding points of the same class within 30 m of each other. Additionally, ground truth points classified as mixed and ambiguous (e.g. class boundaries) were removed. This left 196 points which were used in the accuracy assessment.

The accuracy assessment of classification was carried out by calculating the kappa coefficient in addition to obtaining the overall accuracy using an error matrix (Table 3). Both user's and producer's accuracies were derived, which respectively corresponds to error of commission and omission *(Congalton, 1991).* The kappa value shows the difference between observed agreement of the classification and reference data and therefore the precision of the classification *(Mehner et al, 2004).*

$$Kappa = \frac{NA-B}{N^2-B} \qquad (1)$$

where *A* is the sum of diagonal elements, *B* is the sum of products (row total multiplied by column total) and *N* is the total number of elements in the error matrix (Table 3).

Total accuracy is defined as:

$$Accuracy_{total} = \frac{sum\ of\ diagonals\ in\ the\ error\ matrix}{total\ number\ of\ evaluation\ pixels} \times 100 \qquad (2)$$

2.5.2. Evaluation of model performance

For evaluation of goodness of fit for allometric models and overall model evaluation, statistics such as *RMSE* and R^2 were calculated. For the purposes of model validation, the coefficient of determination (R^2) was preferred owing to the fact that it is useful in regression studies to check how successful the fit is in explaining the variation of the data *(Noone and Vong, 2009)*. It is defined as follows:

$$R^2 = \frac{SSR}{SST} = 1 - \frac{SSE}{SST} \qquad (3)$$

In this equation, *SSR* is the sum of squares of the regression or simply explained variation, which measures the deviation of the observations from their mean:

$$SSR = \sum_{i=1}^{n}(\hat{z}_i - \bar{z})^2 \qquad (4)$$

The *SSE* represents unexplained variation and stands for the sum of squares due to error. This statistic measures the deviation of observations from their predicted values. The closer this value is to 0 the more useful the fit will be for prediction and the smaller the random component of the model is *(MATLAB, 2012)*. It is defined as:

$$SSE = \sum_{i=1}^{n}(z_i - \hat{z}_i)^2 \qquad (5)$$

In equations 4 and 5, $\hat{z}_i$ are the estimated values, $\bar{z}$ is the mean value of measured values and z_i are the measured values. Finally, *SST* is the total sum of squares and presents the total variance of data. It is defined as:

$$SST = SSR + SSE \qquad (6)$$

The coefficient of determination can range from 0 to 1, where values closer to 1 indicate that the regression model was able to explain a greater portion of the variance *(MATLAB, 2012)*.

Another statistic applied in this project was the root mean squared error (*RMSE*), which is a measure of the differences between values predicted by a model and the values actually observed and is defined as:

$$RMSE = \sqrt{\frac{SSE}{n}} \qquad (7)$$

where n is the number of verifying points. Similar to *SSE* statistics, the closer the *RMSE* value is to 0 the more useful a fit is for prediction.

The student's *t-test* was performed for each of the models developed in order to check whether the predicted values of AGB were statistically different from the measured in-the-field AGB values *(Noone and Vong, 2009)*. The *t* statistic gives an idea of how far the prediction is from the truth and was calculated using a two tailed test at the 0.05 significance level as follows:

$$t = \frac{\bar{x}_m - \bar{x}_e}{S_{x_m x_e} \times \sqrt{\frac{2}{n}}} \qquad (8)$$

where $S_{x_m x_e}$ is the pooled standard deviation of measured and estimated AGB values, $\bar{x}_m$ is the mean of measured AGB, $\bar{x}_e$ is the mean of estimated AGB values and n is the sample size.

2.6. Reference biomass estimation

Plot aboveground biomass estimates were obtained by applying species allometric relationships derived from harvested stands in Sweden. In this study, AGB represents the sum

of stem, bark, branch and foliage biomasses *(Zianis et al, 2005).* The DBH parameter alone is commonly used for AGB prediction via allometric equations. However, the inclusion of tree height parameter as another independent variable in the model can improve overall biomass prediction *(Marklund, 1988; Johansson, 1999).* Height-AGB allometric functions were derived only for the dominant tree species in the Skogaryd, which are Norway spruce *(Picea abies),* Scots pine *(Pinus sylvestris)* and Silver birch *(Betula pendula)*. Pine and spruce biomass functions were developed by *Marklund (1988),* while birch allometry was provided by *Johansson (1999)*. In this study, biomass is defined in dry weight terms. The calculation of AGB was based on biomass functions for different tree components *(Zianis et al, 2005)*:

$$AGB = CR + ST \qquad (8)$$

where AGB – total aboveground biomass, CR – crown biomass (branch and foliage biomass) and ST – total stem biomass (stem wood and bark biomass)

Other minor species encountered during fieldwork, such as rowan, were treated as birch. Table 2 shows a summary of equations used for reference biomass estimations.

Table 2. Biomass equations for tree species in Sweden. Number of sampled trees (n), coefficients of determination (R^2), diameter at breast height (DBH) and height (H) of sampled trees *(Zianis et al, 2005).*

	Bio mass (kg)	**DBH**	**H**	**n**	**R^2**	**Equation**	**a**	**b**	**c**	**D**
Spruce	ln(CR)	cm	-	544	0.945	a+b·[D/(D+13)]	-1.2804	8.5242	-	-
Spruce	ln(CR)	cm	m	544	0.949	a+b·[D/(D+13)]+c·H+d·ln(H)	-1.2063	10.9708	-0.0124	-0.4923
Spruce	ln(ST)	cm	-	546	0.988	a+b·[D/(D+14)]	-2.0571	11.3341	-	-
Spruce	ln(ST)	cm	m	546	0.994	a+b·[D/(D+14)]+c·H+d·ln(H)	-2.1702	7.469	0.0289	0.6858
Pine	ln(CR)	cm	-	482	0.901	a+b·[D/(D+10)]	-2.8604	9.1015	-	-
Pine	ln(CR)	cm	m	482	0.922	a+b·[D/(D+10)]+c·ln(H)	-2.5413	13.3955	-1.1955	-
Pine	ln(ST)	cm	-	488	0.978	a+b·[D/(D+13)]	-2.3388	11.3264	-	-
Pine	ln(ST)	cm	m	488	0.99	a+b·[D/(D+13)]+c·H+d·ln(H)	-2.6768	7.5939	0.0151	0.8799
Birch	AGB	mm	-	-	0.985	$a \cdot D^b$	0.00087	2.28639	-	-

2.7. Regression analysis

Thereafter, a regression analysis was carried out in order to describe the relationship between tree height and AGB. The use of DBH parameter was considered to be inappropriate for AGB prediction, as it cannot be directly captured by remote sensing techniques. Moreover, tree height is the only forest parameter that is able to predict biomass estimates, with an accuracy of approximately 85 % *(Papathanassiou et al, 2005)*. Therefore, the task was accomplished by deriving allometric equations, among which the most typical for describing the relation between tree height and biomass is a power function of the form $y = a \times x^c$ *(Mette, 2006).*

Sample size for height-AGB allometry derivation consisted of 189 spruces and 145 pines. A power function fitted well (Figures 8 and 9) and resulted in the following dependencies:

$$AGB_{SPRUCE} = 0.1183 \times H^{2.528} \qquad (9)$$

$$AGB_{PINE} = 0.6696 \times H^{1.996} \qquad (10)$$

Unfortunately, no height measurements of deciduous trees were performed in this study. Therefore, general relations which were empirically derived from forest yield tables for coniferous and broadleaf tree species in Middle Europe were applied for AGB estimation of birch *(Mette et al, 2004):*

$$AGB_{BIRCH} = 0.8 \times H^{1.748} \qquad (11)$$

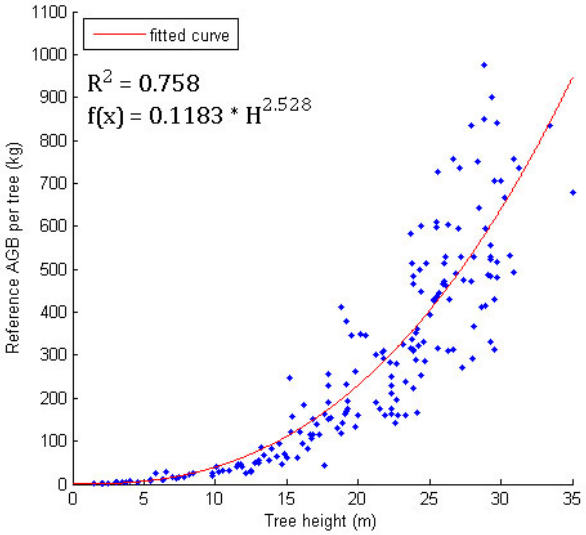

Figure 8. Power model for AGB prediction from LiDAR-derived height estimates for spruce trees.

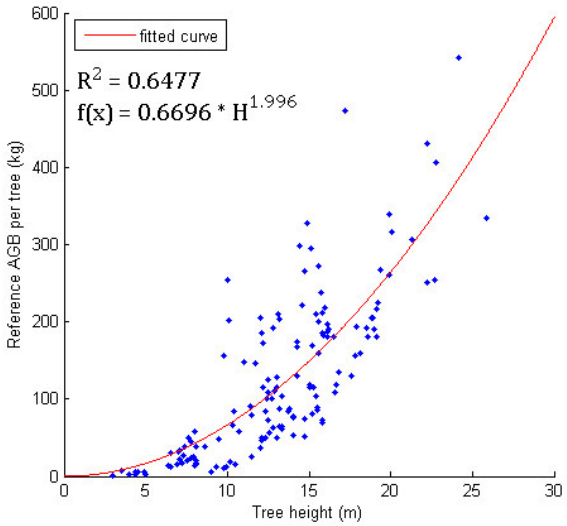

Figure 9. Power model for AGB prediction from LiDAR-derived height estimates for pine trees.

The R^2 values of 0.758 and 0.648 mean that the fit explains 75.8 % and 64.8 % of the total variation in the data about the mean, respectively *(MATLAB, 2012).*

Finally, the vegetation classification was used in conjunction with the CHM for final AGB estimation. Predicted tree canopies with defined heights and species class served as an input for allometric regression models and thus biomass over the area of interest was calculated. AGB was averaged in 10 m by 10 m squares.

3. Results

In this section the outcome of the model developed, with accuracy values, will be presented. All resulting maps are in SWEREF99 coordinate system with following extent, left: 331195, top: 6476475, right: 335975, bottom: 6470075. In addition, maps are overlaid by the WGS 1984 grid, which is more intuitive.

3.1. Reference aboveground biomass estimates

AGB estimates for each of the measured plots in the field can be found in Appendix 1. There was quite substantial variation in biomass observed over the 83 different plots due to age, type and density of the forest. By knowing the total amount of AGB in each of the surveyed plots in the field, it was also possible to determine average AGB over each of these plots in kg/m^2. AGB varied from 2.5 kg/m^2 in very young sparse forest stands to 44 kg/m^2 in mature dense forest stands.

By using measured data in the field it was also possible to determine the percentage of AGB over plots corrected for different tree height and DBH ranges. Across surveyed plots only 0.1 % of biomass was present in trees below 2 m in height and 3 cm in DBH, reaching a maximum of 5 % in dense young forest. On the other hand, 0.7 % of AGB was present in trees below 3 m in height and 4 cm in DBH with a maximum of 25 % in dense young forest. Therefore, it was decided that application of the algorithm for canopy extraction with a height threshold of 2 m should be satisfactory over the whole area of study. The application of such a threshold would potentially account for 99.9 % of the AGB in the coniferous dominant forest.

The number of trees measured in the field plots varied substantially depending on forest type and ranged from only 6 trees per plot in sparse mature forest to more than a hundred in highly dense young forest (Appendix 1).

3.2. Vegetation classes

The final map of vegetation types based on maximum likelihood classification to be found in the Skogaryd area is presented in Figure 10. According to the classification performed, the dominant species in the area are spruce and pine, which both occupy equal areas of 7.9 km^2. In contrast, deciduous forest takes up only 4.6 km^2 and is mostly found in inhabited areas.

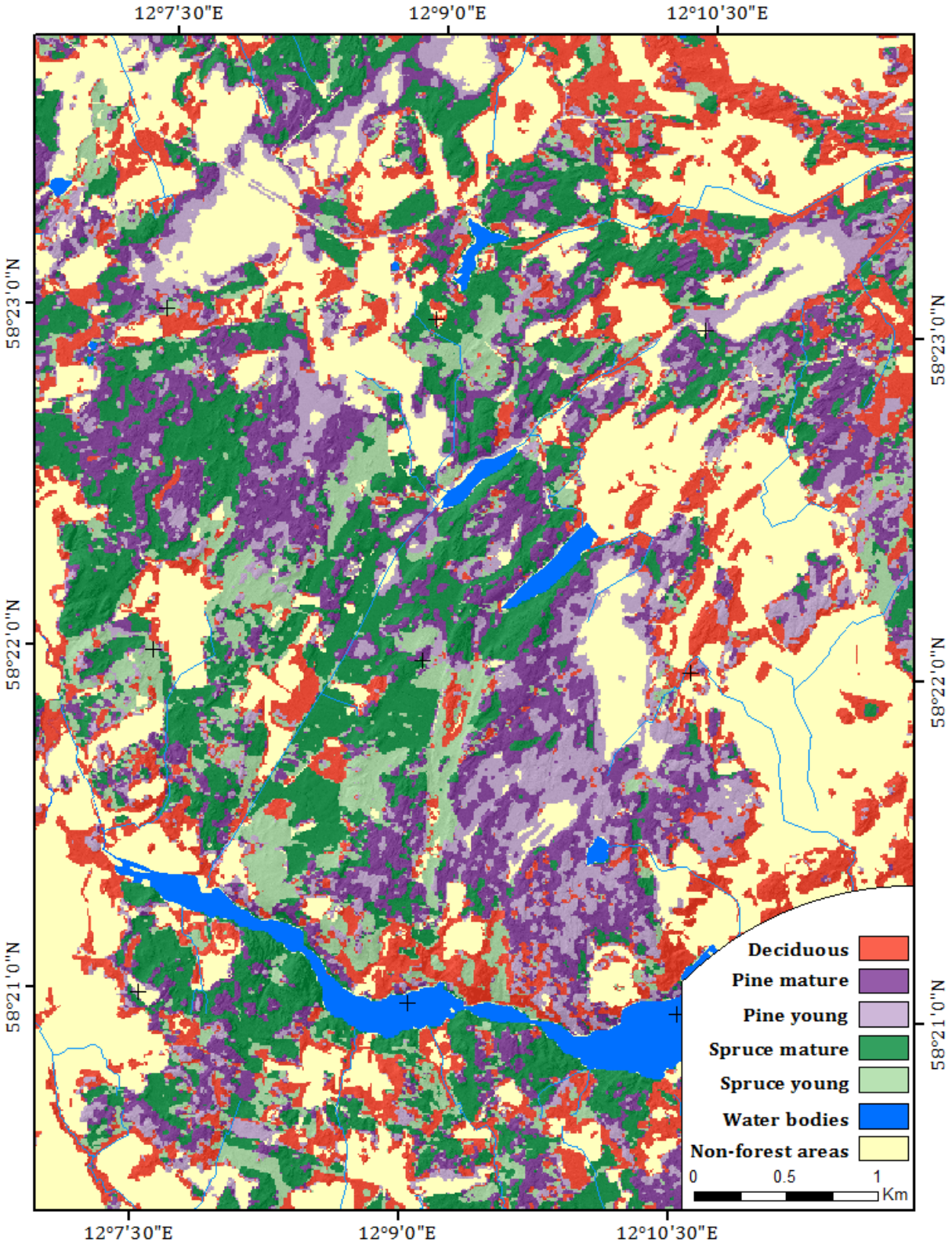

Figure 10. Vegetation map from SPOT-5 data for July 2011 (10 m pixel resolution). Water bodies layer was provided by: *@ Lantmäteriet, Dnr: i2012/927*

The error matrix of this classification including user's and producer's accuracies is presented in Table 3. In addition, kappa coefficient and total accuracy were calculated to be as follows:

$$Kappa \approx 0.75$$

$$Accuracy_{total} \approx 81\ \%$$

Table 3. Error matrix for vegetation classes.

	Spruce Mature	Spruce Young	Pine Mature	Pine Young	Deciduous	Totals	User's	Producer's	Area (km^2)
Spruce Mature	67	3	5	0	1	76	88 %	92 %	5.4
Spruce Young	2	25	3	0	1	31	81 %	86 %	2.5
Pine Mature	4	1	32	8	0	45	71 %	68 %	4.6
Pine Young	0	0	7	10	0	17	59 %	50 %	3.2
Deciduous	0	0	0	2	25	27	93 %	93 %	4.6
Totals	73	29	47	20	27	**196**			

As it can be seen from the error matrix above the main misclassification occurred among pine young and pine mature classes, while all the other classes were identified with accuracies higher than 80 %.

3.3. LiDAR-derived forest inventory parameters

In general, the number of trees identified by the CHM segmentation algorithms has not corresponded to the number of trees measured in the field. As expected, there was a huge overrepresentation of trees when using local maximum algorithm with 2 m by 2 m evaluation window, while the same approach with a larger window resulted in underrepresentation of tree canopies. The IWS showed the best delineation of tree canopies across young forest. It was able to identify on average 68 % of trees measured during fieldwork in the young forest stands, while mature forests remained largely overrepresented.

Regression analysis was carried out to investigate the relationship between LiDAR-derived and measured tree heights over the measured field plots. Figures 11 and 12 show the mean and maximum heights calculated from the CHM plotted against field canopy heights. The 1:1 line shows the perfect match between measured and estimated values. In addition, the impact of GPS accuracy on the relationship is depicted in the form of a range of LiDAR-derived tree heights in a radius of 5 m from the plot center. Considering, that it was impossible to correlate tree heights of individual trees it is assumed that the mean and maximum statistics of tree height over each plot should provide good information for tree height validation.

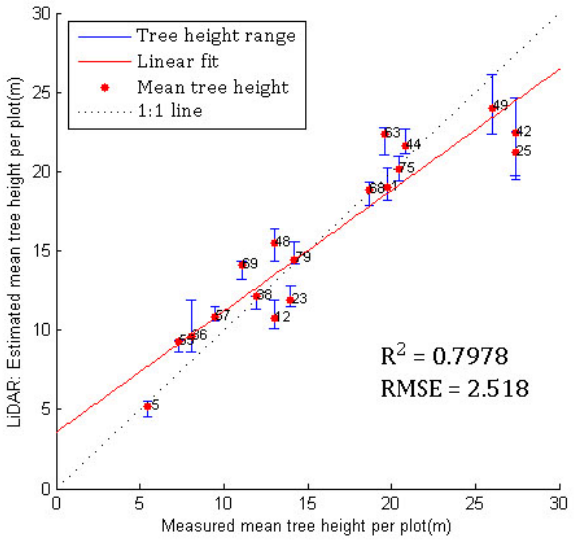

Figure 11. Predicted vs. field-measured mean tree height per plot. Numbers correspond to the plots measured in the field (see Appendix 2).

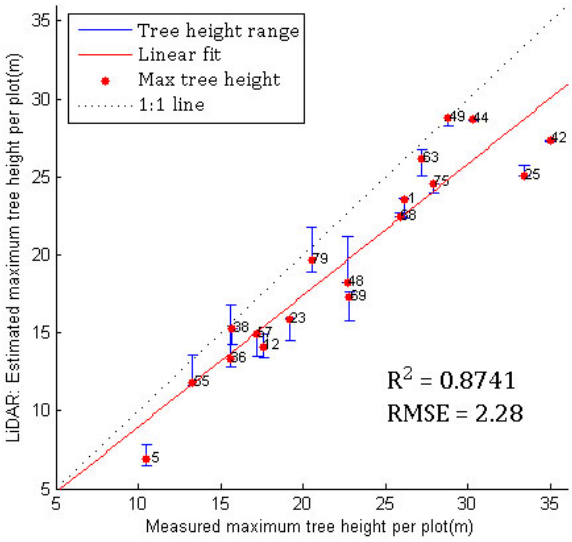

Figure 12. Predicted vs. field-measured maximum tree height per plot. Numbers correspond to the plots measured in the field (see Appendix 2).

As can be seen from Figure 12 above, there is substantial underestimation of the highest trees. On average, this is about 14 % and ranges from 0.2 % to 34 %. The comparison of mean tree height measured in the field against LiDAR-derived heights resulted in slightly worse correlation with no clear underestimation.

3.4. Aboveground biomass estimates over the study area

The comparison of LiDAR-derived AGB with the "in situ" aboveground biomass measurements revealed the most accurate segmentation algorithm. Surprisingly the best AGB prediction was achieved when using a local maximum algorithm with a constant 3 m by 3 m evaluation window, as can be seen in Figure 14. In contrast, there was a huge overestimation of AGB when using a 2 m by 2 m evaluation window, showing that an approximation of 4 m^2 for individual tree crowns over the area is inappropriate. Significant LiDAR biomass overestimation occurred in 86 % and underestimation occurred only in 7% of the plot comparisons (Figure 13).

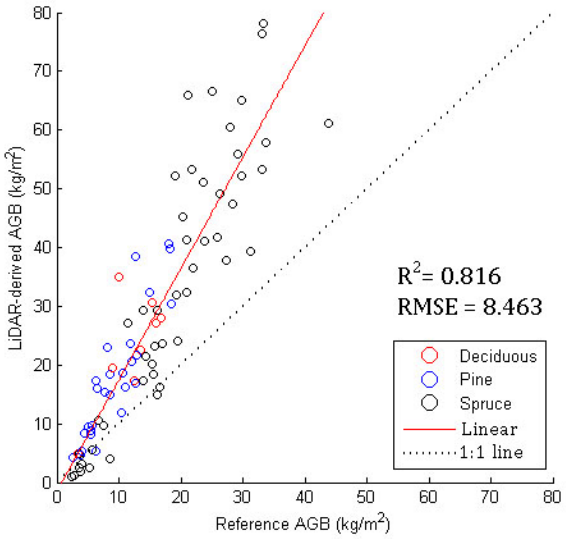

Figure 13. Field-measured vs. predicted AGB using local maximum algorithm with constant 2m by 2m evaluation window.

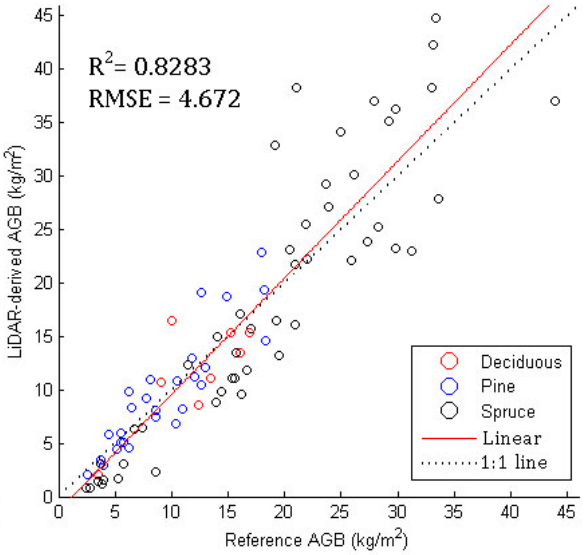

Figure 14. Field-measured vs. predicted AGB using local maximum algorithm with constant 3m by 3m evaluation window.

Estimation of AGB using the IWS approach gave similar results as the local maximum algorithm with a constant 3 m by 3 m evaluation window, though with slightly worse statistical accuracy. The main misestimation when using IWS occurred in the spruce dominated plots (Figure 15).

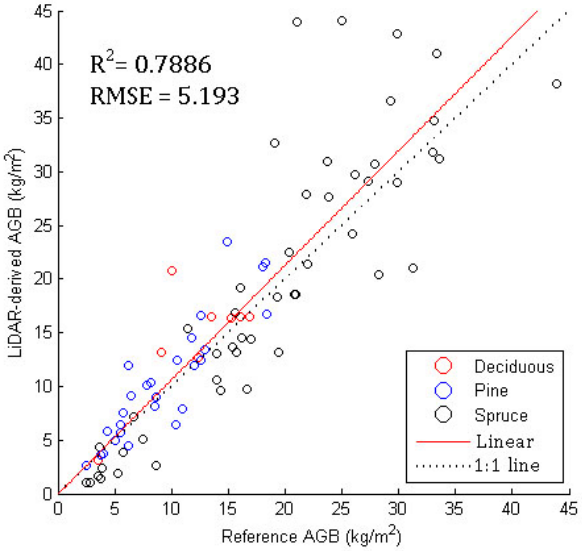

Figure 15. Field-measured vs. predicted AGB using inverse watershed segmentation (IWS) algorithm.

A *t-test* revealed that estimated values of AGB using both local maximum with a 3 m by 3 m window size and IWS segmentation algorithms were not significantly different from measurements of AGB in the field at the 0.05 significance level. In case of local maximum with a 2 m by 2 m window size the null hypothesis was rejected, as the *p value* was significantly smaller than 0.05.

Although inverse watershed segmentation was not able to improve AGB estimation as compared to a local maximum algorithm with a constant 3 m by 3 m evaluation window, it

was expected to at least produce better results for young forest. In Figures 16 and 17 the comparison of the above approaches over young forests is shown. Surprisingly enough, both methods showed similar results, proving that IWS was not able to better delineate small canopies in young forest stands.

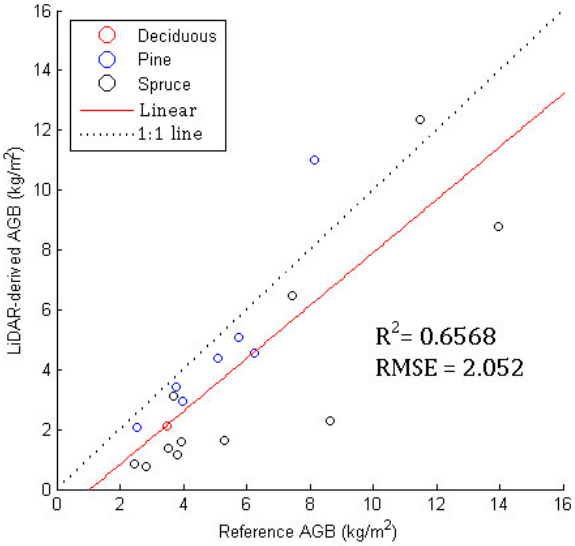

Figure 16. Field-measured vs. predicted AGB in young forest using local maximum algorithm with constant 3m by 3m evaluation window.

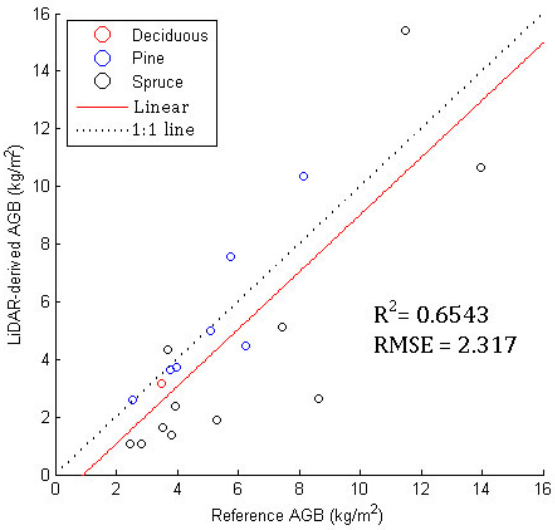

Figure 17. Field-measured vs. predicted AGB in young forest using inverse watershed segmentation (IWS) algorithm.

The final aboveground biomass map using the best model derived for June 2011 is presented in Figure 18. The biomass was predicted to vary from 0.01 to 93.5 kg/m^2. However, it is important to note that the mean AGB in the area was equal to 9.4 kg/m^2 with standard deviation of 9.2 kg/m^2 and that extreme values of more than 50 kg/m^2 were quite rare and occupied only 1 % of the area.

Overall, the Skogaryd area is characterized by a patchy AGB distribution with high values of more than 50 kg/m^2 located strictly in mature spruce forest stands as identified by the performed vegetation classification. Also, considering that forest AGB in this study is a function of tree height and the number of trees per unit area, the resulting AGB map in Figure 18 is well correlated with the CHM in Appendix 5.

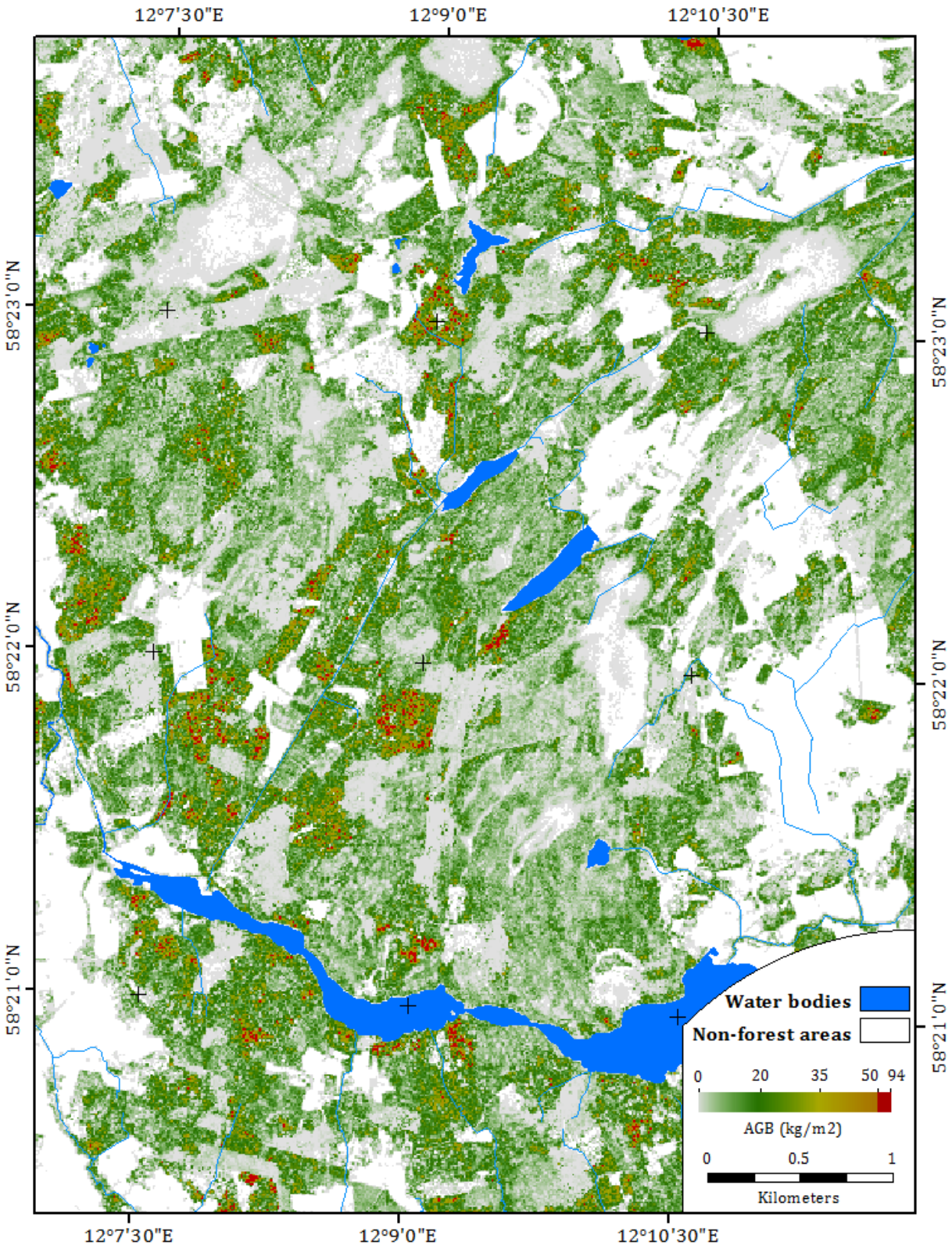

Figure 18. Aboveground biomass map for June 2011 over the Skogaryd area based on a using local maximum algorithm with a constant 3 m by 3 m evaluation window approach (R^2 = *0.83*) (10 m pixel resolution). Water bodies layer was provided by: *@ Lantmäteriet, Dnr: i2012/927.*

4. Discussion

In this section, the effectiveness of the method applied for the estimation of AGB over the studied region as well as possible sources of uncertainties will be discussed.

4.1. Effectiveness of the vegetation classification

The result of 0.81 for the total accuracy of the maximum likelihood classification can be considered acceptable or even good for optical types of data. Although there was a time gap of one year between the satellite data acquisition and the ground-truthing carried out, it has a presumably minor effect on the classification performed. The average speed of height growth for coniferous forest is roughly 30 cm per year (*Lieffers et al, 1996*). Therefore the time gap of one year may be considered as negligible in terms of forest age structure change. On the other hand, the Skogaryd area is comprised of forest stands that are significantly influenced by human activity and a rapid change of land cover between 2011 and 2012 was observed in many places, e.g. due to clear-cutting and thinning of forests. The influence of land cover change was completely avoided owing to the feature extraction procedure.

With regards to the spectral separability of the different vegetation types, the main issue was that pine mature and pine young forests were often misclassified. This might have been caused by substantial spectral overlap between those classes. It is most probably caused by the density of the forest influencing the spectral signature in areas of pine stands. In addition, during the fieldwork, it was noticed that a lot of pine forest stands were located in wetlands, which influenced the growth of trees. Therefore, such mature pine forest stands might feature spectral properties similar to young pine forest. Another consideration when assessing the classification output was the influence of shrub and ground layers on the spectral separability of vegetation classes. This is an issue especially in sparse forest stands, where ground layer is visible to the satellite sensor. Consequently bare earth with certain degrees of stoniness creates mixed pixel values together with green vegetation leading to a large standard deviation for each of the vegetation classes.

In general, the spectral similarity among green tree vegetation posed a severe problem to the classifier. In Figures 19 and 20 spectral scatter plots for classified SPOT-5 image bands are presented, where the means (crosses) and two standard deviations from the mean (ellipses) of training areas are also shown. On these figures colors correspond to the frequency of occurrence for a particular pixel value pair. Pixel pairs colored in magenta have a low frequency of occurrence while those colored in red have a high frequency, with several colors in between. The axes are in DN (digital number), which is closely related to reflectance values. It is clearly seen that there is substantial overlapping between training areas of vegetation classes in terms of spectral characteristics. It is especially pronounced when comparing red and near-infrared (NIR) bands, while differentiation between NIR and middle-infrared (MIR) bands provides the best separability of vegetation classes.

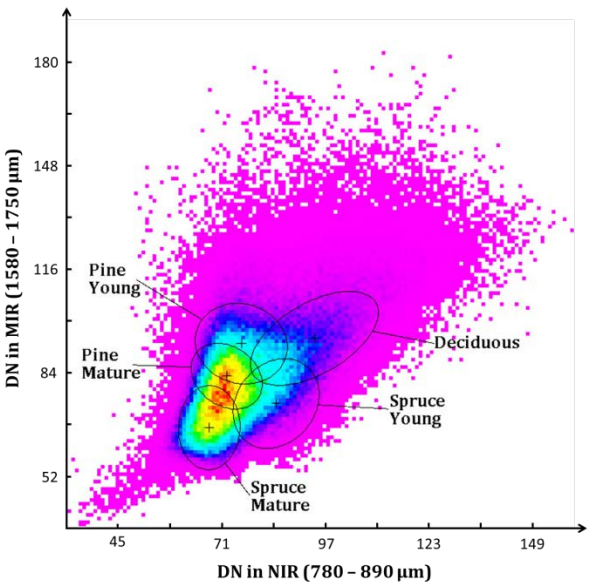

Figure 19. NIR-MIR spectral scatter plot.

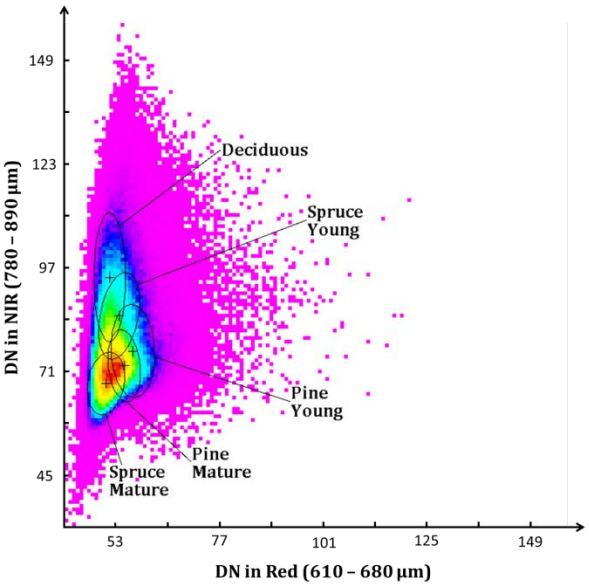

Figure 20. Red-NIR spectral scatter plot.

A possible solution for classification improvement is to assign an additional class for mixed forest based on training areas identified from ground truth data. Whether a trial-and-error based rearranging of training areas could have improved the overall results remains speculative. Regardless, the significant spectral overlap is inherent among the different types of green vegetation and all forest types can still be identified reliably, being only a little underclassified or overclassified.

4.2. LiDAR-derived tree metrics uncertainties

The algorithm developed in this study for LiDAR analysis was able to classify tree canopies with its subsequent segmentation into distinct trees. These outputs were crucial in prediction of individual tree heights and thus AGB. Uncertainties in obtaining forest inventory parameters from LiDAR data may be related firstly to the nature of LiDAR measurements and secondly to introduction of errors during processing.

Numerous studies (*Gaveau and Hill, 2003; Bortolot and Wynne, 2005; Lewis and Hancock, 2007*) have examined main factors influencing the derivation of tree parameters from discrete-return LiDAR data. Firstly, it is uncertain that a laser beam from the sensor will strike the top of the tree. Secondly, there is a chance that a laser beam will penetrate through the tree canopy before being reflected. Lastly, there is no assurance that a laser beam will strike the actual ground surface (*Bortolot and Wynne, 2005*). For example, errors in LiDAR-derived height estimates could have been caused by ground vegetation which was registered as ground returns *(Lantmäteriet, 2012).* All these factors are valid for the measurement unit (Leica ALS50-II) used for LiDAR surveying in this study and could lead to the observed underestimation of the tree height. In addition, the Leica ALS50-II system has a beam divergence of 0.22 mrads, meaning that the size of the sensor's footprint at an altitude of 2000 m was around 50 cm. The relatively small footprint of the LiDAR sensor implies that there was a higher chance of complete beam absorption by the tree canopy before it reached the ground and that the beam return represents blurred records of tree height over the sensor's

footprint area. In contrast, it also implies a higher chance for a beam to penetrate holes in the vegetation canopy, thus providing ground samples *(Lewis and Hancock, 2007).* Another issue to be considered is the point density of the LiDAR dataset, which was relatively low (~0.8 points/m^2), and therefore the chance of a point actually striking the very top of a tree was also low. This effect is particularly pronounced for trees with a large crown diameter *(Ireland, 2011).* Increasing sampling density can therefore result in model improvement.

Validation of the model applied showed a tree height underestimation of around 14% when comparing maximum measured and predicted heights over plots. This underestimation could be due to the nature of the discrete-return LiDAR scanning as explained above and presents evidence of a limitation in the algorithm. Previous studies also indicate significant underestimation of the field-measured height in coniferous trees by LiDAR *(Morsdorf et al, 2004; Andersen, 2009).* Unfortunately, it was impossible to investigate the individual contribution of the factors mentioned above due to the lack of information on undergrowth in the Skogaryd and the echo-triggering mechanism of the system used for LiDAR measurements *(Ireland, 2011).*

There was also uncertainty embedded in the LiDAR dataset in the form of measurement accuracy. According to the Swedish Land Survey, the vertical precision of the individual laser points was in general better than 10 cm on planar, open surfaces. However, locally precision and accuracy varied significantly depending on slope steepness and terrain accessibility. For example, in areas with dense forest the point density on the ground decreases, which leads to the loss of small terrain formations. On the other hand, the horizontal precision of the individual laser points was even lower – around 30 cm – which decreased further with increasing slope steepness *(Lantmäteriet, 2012).*

Another important source of error when estimating AGB was due to shortcomings in the processing of the LiDAR data. The classification of raw LiDAR data was performed using automated methods, which are far from perfect. For example, such objects as power lines might have been classified as high vegetation leading to overclassification of biomass in the area. In areas of dense low vegetation the laser points could have been classified as ground, although they actually represent grass level. Some points of building edges remained to be classified as high vegetation. Thus, classification is never flawless and a small amount of points will always be assigned to the wrong class *(Lantmäteriet, 2012).* This led to errors in both the DSM and the DTM, and eventually the CHM, which was difficult to detect even in manual reviews.

4.3. Individual tree approach

Estimation of AGB at an individual tree level using LiDAR data is highly dependent on successful canopy detection and characterization. In turn, the accuracy of individual tree identification depends on the point density of LiDAR data and the segmentation algorithm applied and is lower in dense and heterogeneous forests *(Li et al, 2012).* Generally, methods developed in this field can only detect dominant trees in the upper canopy with relatively good accuracies *(Edson and Wing, 2011).*

In this study two different types of CHM segmentation were applied. It was expected that IWS would provide an advantage over a local maximum algorithm with a constant 3 m by 3 m evaluation window. In the latter method, the maximum height tree point per cell is extracted, which potentially underestimates the number of trees in dense and especially young forest stands. According to previous studies, IWS was able to identify individual trees in some forest types *(Andersen, 2009).* It is efficient in coniferous forests, but usually fails in deciduous forests by mixing trees into one watershed, or in forests where sub canopy is hidden under major canopy. However, this is the case with the majority of CHM based approaches for tree modeling *(Edson and Wing, 2011).*

Initial constraints for local maximum algorithms have strongly affected the resultant AGB estimates. For example, a 2 m by 2 m window size proved to be inappropriate, especially for delineating individual trees in mature forest. The overrepresentation of tree crowns occurred due to approximation of tree crowns to the size of the constant window used and eventually led to overestimated AGB values. This is evident considering the average canopy width for mature coniferous trees is equal to 3 - 5 m *(Kantola and Mäkelä, 2004).*

The IWS from the SAGA GIS software was not able to identify individual trees and thus give an AGB estimate with accuracies higher than that of the local maximum method. When using both methods, the output tree crowns in mature forests were relatively overrepresented, while underrepresentation took place in young forests. This was fed into the AGB prediction process and caused the misestimates observed. Though application of the local maximum approach for delineation of individual tree canopies resulted in better correlation, many trees were still missed and others were mixed into one canopy. The application of local maximum with a variable-size window approach for CHM segmentation might resolve this issue.

4.4. Aboveground biomass estimation over the study area

The approach used for AGB estimation through LiDAR-derived tree heights is mainly based on previous studies, which proved tree height to be the most reliable parameter in AGB prediction *(Mette et al, 2004; Papathanassiou et al, 2005).* Established relationships between AGB and LiDAR-derived tree heights approximated the first order power function, which led to the introduction of errors into the AGB calculation. As can be clearly seen from Figure 9, the model developed for biomass prediction in pine produced highly-overestimated values of AGB among young trees. Moreover, the uncertainty in AGB prediction grows with increasing canopy height owing to the small sample size of the highest trees. Nevertheless, the ability of LiDAR-derived tree heights to predict AGB may be considered as quite strong. The regression analysis showed relatively good goodness of fit statistics for predicting aboveground biomass in pine and spruce trees, with R^2 values of 0.65 and 0.76, respectively.

The main parameters used for AGB estimation across surveyed plots were DBH and tree height. It was suggested that the use of both these parameters would result in improved AGB estimates. However, as shown in *Jonsson (1999)* and *Marklund (1988)* the introduction of a tree height variable leads to less than 1 % increase in the R^2 value of the prediction models.

Thus, the absence of height measurements for the majority of plots introduces a minor error into the prediction of AGB.

After investigation of allometric models used in this study for AGB estimation, it was found that AGB is highly dependent on tree species. This dependence can particularly be observed between coniferous and deciduous species, though the relation used in this study for the estimation of AGB in deciduous trees represents a generalized relationship developed for both broadleaf and coniferous species. For example, as can be seen from the figure below, the difference in AGB estimates for coniferous and deciduous 20 m high trees was around 200 kg. The estimates for deciduous trees might be improved by deriving AGB-height allometry equations from the relationship between DBH and height as shown in *Mehtätalo (2005)*. Comparison of height-biomass allometric relationships for different tree species used in this study is presented in Figure 21.

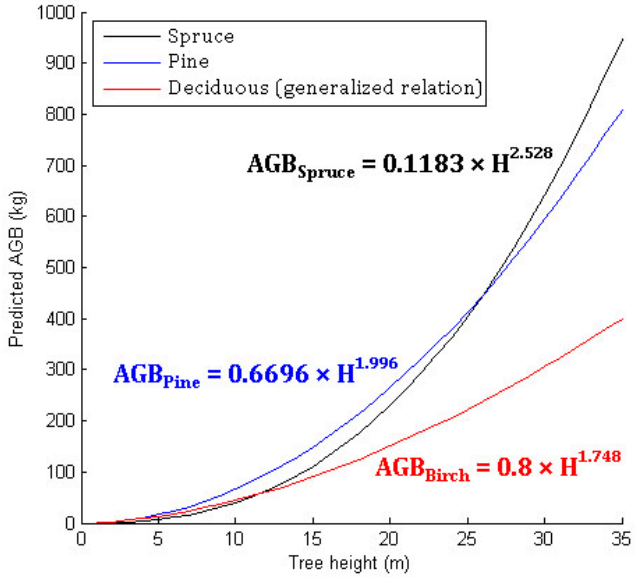

Figure 21. Height-biomass allometric relationships developed in this study using regression analysis.

The equations derived in this study for AGB prediction were successfully applied over the whole area of study, showing the model's good predictive ability. However, when separating the young forest from mature areas, the model demonstrated lower performance, owing to flaws in the tree segmentation algorithms and the relatively low point density of the LiDAR dataset. Indeed, the ability of low-density LiDAR to detect small trees or trees hidden under the canopies of high trees is usually less accurate due to the smaller size of the crown. The accuracy of detection is also worsened due to the proximity of returns from smaller trees to ground returns. Nevertheless, young forest stands with small crowns play an important role in carbon cycling and determination of AGB *(Ireland, 2011)*.

There were, of course, other uncertainties related to AGB estimation over the study area. Firstly, the time gap between the LiDAR survey and the fieldwork was more than a year, which means that any forest disturbance in the form of clear-cutting, thinning or storms might affect the output. For example, during fieldwork it was noticed that plot #53 contained a relatively large amount of stumps. This has an effect on the LiDAR-derived biomass estimate,

which was double the amount of AGB measured in the field. This suggests that there was thinning performed in this area between summers 2011 and 2012. Secondly, substantial numbers of trees in the studied area were without tops, most likely due to a recent storm. According to Swedish mass media, the remnants of Hurricane Katia in September 2011 battered Sweden, especially Västra Götaland County, with strong winds of up to 24 m/s. SMHI issued a class 1 warning. The storm caused significant forest damage in the area of study, as a lot of trees were blown down or lost their treetops *(The Local, 2011).* Thirdly, approximately 75 % of the data available should have been used in the process of model development and the rest held back for validation *(Smith and Smith, 2007).* Nevertheless, in this study the whole set of field tree height data was used in order to evaluate the regression relationships. This was done due to time constraints during fieldwork which limited the number of validation points. Finally, as the averaged LiDAR-derived tree heights were underestimated by 14%, there was also an underestimation of AGB across the whole area of study as the tree heights derived from LiDAR data were not corrected.

Although many studies have successfully been able to extract forest inventory parameters at individual tree level from LiDAR data using automatic computer algorithms *(e.g. Morsdorf et al, 2004; Bortolot and Wynne, 2005; Edson and Wing, 2011)*, results are usually presented at stand or plot levels *(Popescu, 2007).* This made it complicated to compare the outcome of biomass calculations in this study in kg/m^2 to other estimates of aboveground biomass over similar types of forest. A good comparison can be made between this study and research made by the Woods Hole Research Center and the U.S. Geological Survey, who have been able to create a forest map of the USA based on satellite radar and optical sensors and a huge amount of ground-based data *(NASA, 2012).* For instance, the detailed map of conifer-dominated forests of the Pacific Northwest provides values of AGB estimates ranging from 0 to 60 kg/m^2 as compared to 0 to 94 kg/m^2 in the Skogaryd. However, it is important to note that AGB in their study was mapped down to 30 m in contrast to 10 m in this study.

4.5. GPS accuracy assessment

The readouts of GPS accuracy measurements in the field varied from 4 m to 6 m. When performing analysis for the best derived models it was decided to shift 15 m by 15 m plots within a 5 m radius and examine how much of the uncertainty might be involved in AGB estimation due to GPS unit constraints. As can be seen from Figures 22 and 23, there are plots which can be considered heterogeneous with biomass change of more than 20 %.

The absolute values of standard deviation are of course higher in mature forest plots, while relative values of this parameter are more attributable to young forest plots. Considering the methodology applied, this suggests that young forest plots measured in the field were characterized by lower homogeneity as compared to mature forest plots.

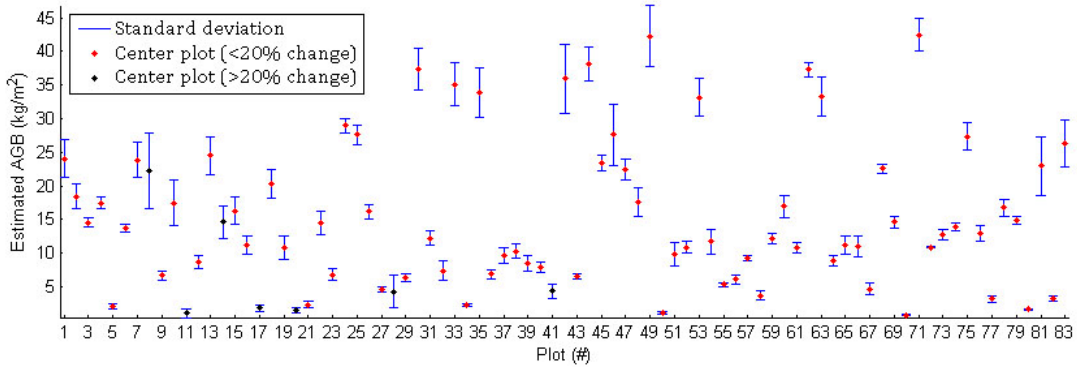

Figure 22. GPS accuracy assessment when using local maximum algorithm with constant 3 m by 3 m evaluation window.

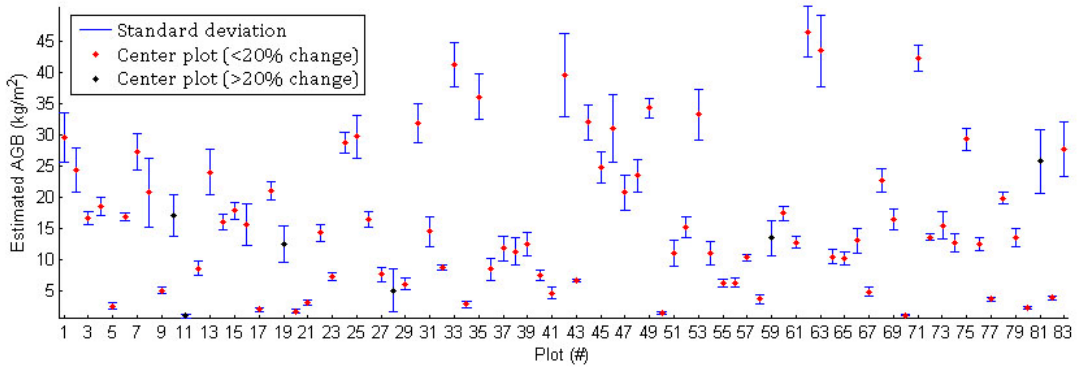

Figure 23. GPS accuracy assessment when using watershed segmentation (IWS) algorithm.

An exclusion of relatively heterogeneous plots from model validation might produce better results. However, there is no assurance that this heterogeneity is caused by GPS inaccuracy only. Imperfect tree segmentation algorithms might present another significant cause of over- or underrepresentation of trees in plots.

5. Conclusions

This project was performed as a baseline for future work on GHG exchange in the Skogaryd area within the frame of the LAGGE project. The robust estimate of AGB for conifer-dominated forest in Västra Götaland County using a fusion of discrete-return airborne LiDAR and satellite imagery is given, which proves the validity of the methodology applied. Results show AGB to vary from less than 1 kg/m^2 in very young forests up to 94 kg/m^2 in mature spruce forests with *RMSE* of 2 kg/m^2 and 4.7 kg/m^2, respectively.

With respect to the first hypothesis, the analysis based on SPOT-5 data was able to provide an accurate mapping of tree species and thus may be used for classification of LiDAR-derived CHM. With respect to the second hypothesis, LIDAR data proved to be useful for AGB estimation through the use of allometric relationships. Using a local maximum algorithm with a constant 3 m by 3 m evaluation window method gave the most accurate prediction of AGB (R^2 = 0.83), with the lowest *RMSE* value. It is shown that the introduction of watershed segmentation does not improve the result (R^2 = 0.79).

Availability of baseline AGB estimates allows further monitoring of this forest ecosystem for disturbance and change, though an extensive program of flights is required in order to collect adequate amounts of data. Furthermore, AGB values can be directly used in further studies of carbon stocks in the Skogaryd, assuming carbon to be 45 % of total biomass following *Whittaker (1975).*

Potentially, the algorithm developed in this study may be used for assessment of individual tree components of biomass, such as foliage or stem wood, since allometry for tree components is readily available. Moreover, intermediate results derived in this study, such as DTM and DSM models, are also valuable in forest applications. The DTM in itself is quite helpful for planning and operational activities, while the DSM alone delineates vegetation structure and thus may be used for understanding forest roughness.

For further research in this field it is suggested to fully explore the potential of other algorithms for individual tree segmentation, the use of which can potentially provide an improved baseline estimate of AGB. However, in order to accurately validate such segmentation the precise position of each tree in the field should be measured, which is only possible by using differential GPS unit. It would also be useful to test if the model for AGB prediction in this study would be effective in other parts of Sweden.

References

Andersen, H.-E. (2009): Using Airborne Light Detection and Ranging (LiDAR) to characterize forest stand condition on the Kenai Peninsula of Alaska. Western Journal of Applied Forestry, 24, 95 – 102

Bortolot, Z. J. and Wynne, R. H. (2005): Estimating forest biomass using small footprint LiDAR data: An individual tree-based approach that incorporates training data. ISPRS Journal of Photogrammetry & Remote Sensing, 59, 342 – 360

Chen, Q., Laurin, G. V., Battles, J. J. and Saah, D. (2012): Integration of airborne LiDAR and vegetation types derived from aerial photography for mapping aboveground live biomass. Remote Sensing of Environment, 121, 108 – 117

Congalton R. G. (1991): A Review of Assessing the Accuracy of Classifications of Remotely Sensed Data. Remote Sensing of Environment, 37, 35 – 46

Edson, C. and Wing, M. G. (2011): Airborne Light Detection and Ranging (LiDAR) for Individual Tree Stem Location, Height, and Biomass Measurements. Remote Sensing, 3, 2494 – 2528

Evans, J. S., Hudak, A. T., Faux, R. and Smith, A. M. S. (2009): Discrete Return LiDAR in Natural Resources: Recommendations for Project Planning, Data Processing, and Deliverables. Remote Sensing, 1, 776 – 794

Gaveau, D. A. and Hill, R. S. (2003): Quantifying canopy height underestimation by laser pulse penetration in small-footprint airborne laser scanner data. Canadian Journal of Remote Sensing, 29, 650 – 657

Hese, S., Lucht, W. and Schmullius, C. (2005): Global biomass mapping for an improved understanding of the CO_2 balance - the Earth observation mission carbon-3D. Remote Sensing of Environment, 94, 94 – 104

Houghton, R. A. (2005): Aboveground Forest Biomass and the Global Carbon Balance. Global Change Biology, 11, 945 – 958

Houghton, R. A., Hall, F. and Goetz, S. J. (2009): Importance of biomass in the global carbon cycle. Journal of geophysical research, 114, 1 – 13

IPCC (2007): Climate Change 2007: Mitigation of Climate Change. IPCC Fourth Assessment Report (AR4). Contribution of Working Group III to the Fourth Assessment Report of the Intergovernmental Panel on Climate Change, 2007: Metz, B., Davidson, O. R., Bosch, P. R., Dave, R. and Meyer L. A. (eds). Cambridge University Press, Cambridge, United Kingdom and New York, NY, USA

Ireland, L. (2011): Estimating biomass of mountain birch in Fennoscandia using discrete return airborne LiDAR. Master's Thesis in Remote Sensing at the Department of Civil, Environmental and Geomatic Engineering, University College London

Jochem, A., Hollaus, M., Rutzinger, M. and Höfle, B. (2011): Estimation of Aboveground Biomass in Alpine Forests: A Semi-Empirical Approach Considering Canopy Transparency Derived from Airborne LiDAR Data. Sensors 2011, 11, 278 – 295

Johansson, T. (1999): Biomass equations for determining functions of pendula and pubescent birches growing on abandoned farmland and some practical implications. Biomass and Bioenergy, 16, 223 – 238

Kantola, A. and Mäkelä, A. (2004): Crown development in Norway spruce (Picea abies (L.) Karst.). Trees, 18, 408 – 421

Lefsky, M. A., Cohen, W. B., Harding, D. J., Parker, G. G., Acker S. A. and Gower S. T. (2001): LiDAR Remote Sensing of Aboveground Biomass in Three Biomes. International Archives of Photogrammetry and Remote Sensing, Volume XXXIV-3/W4 Annapolis, MD

Lewis, P. and Hancock, S. (2007): LiDAR for vegetation applications, UCL, Gower St, London, UK

Li, W., Guo, Q., Jakubowski, M. K. and Kelly, M. (2012): A New Method for Segmenting Individual Trees from the Lidar Point Cloud. Photogrammetric Engineering & Remote Sensing, 78(1), 75 – 84

Lieffers, V. J., Stadt, K. J. and Navratil, S. (1996): Age structure and growth of understory white spruce under aspen. Canadian Journal of Forest Research, 26(6), 1002 – 1007

Marklund, L. G. (1988): Biomassafunktioner för tall, gran och björk i Sverige. Sveriges lantbruksuniversitet, Institutionen för skogstaxering, Rapport 45, 1 – 73

Mehner, H., Cutler, M., Fairbairn, D. and Thompson, G. (2004): Remote sensing of upland vegetation: the potential of high spatial resolution satellite sensors, Global Ecology and Biogeography, 13, 359 – 369

Mehtätalo, L. (2005): Height-Diameter Models for Scots Pine and Birch in Finland. Silva Fennica, 39(1), 55 – 66

Mette, T., Papathanassiou, K., Hajnsek, I. (2004): Biomass estimation from polarimetric SAR interferometry over heterogeneous forest terrain. Geoscience and Remote Sensing Symposium, 2004. IGARSS '04 Proceedings, IEEE International, 511– 514

Mette, T. (2006): Forest Biomass Estimation from Polarimetric SAR Interferometry. Dissertation for Doctor of Science, Center of Life and Food Sciences Weihenstephan, Technical University of Munich

Morsdorf, F., Meier, E., Kötz, B., Itten, K. I., Dobbertin, M. and Allgöwer, B. (2004): LIDAR-based geometric reconstruction of boreal type forest stands at single tree level for forest and wildland fire management, Remote Sensing of Environment, 92, 353 – 362

Noone, K. J. and Vong, R. J. (2009): Statistics for the Geosciences, Version: Autumn 2009, Department of Applied Environmental Science, Stockholm University

Peckham, R. J. and Gyozo, J. (2007): Development and Applications in a Policy Support Environment Series: Lecture Notes in Geoinformation and Cartography, Heidelberg, Germany

Popescu, S. C. (2007): Estimating biomass of individual pine trees using airborne LiDAR. Biomass and Bioenergy, 31, 646 – 655

Smith, J. and Smith, P. (2007): Environmental modelling – an introduction. Oxford University Press Inc. New York, United States

Whittaker, R. H. (1975): Communities and Ecosystems. MacMillan Publishing, New York, United States

Online resources:

ESRI (2011): LiDAR Analysis in ArcGIS 10 for Forestry Applications, Esri Publications, available at: *http://www.esri.com/library/whitepapers/pdfs/lidar-analysis-forestry-10.pdf*, accessed: 12 December 2012

Haglöf (2012): Vertex IV and Transponder T3 manual (English), available at: *http://www.haglofcg.com/index.php?option=com_docman&task=cat_view&gid=51&lang=en*, accessed: 06 October 2012

Lantmäteriet (2012): Produktbeskrivning: Laserdata, available at: *http://www.lantmateriet.se/Global/Kartor%20och%20geografisk%20information/H%C3%B6jddata/Produktbeskrivningar/laserdat.pdf*, accessed: 12 December 2012

MATLAB (2012): MatLab R2012b documentation. Evaluating Goodness of Fit, available at: *http://www.mathworks.se/help/curvefit/evaluating-goodness-of-fit.html*, accessed: 23 October 2012

Merrick & Company (2012): Mars Explorer HELP File, available at: *http://www.merrick.com/site/static/mars/documentation/MARS_v7.0_Help.pdf*, accessed: 29 September 2012

Muise, A. (2011): Raster Image Processing Tips and Tricks — Part 4: Image Classification. ArcGIS Resources, available at: *http://blogs.esri.com/esri/arcgis/2011/01/10/georef4/*, accessed: 15 October 2012

NASA (2012): Closeup on forests of the Pacific Northwest. Visible Earth: A catalog of NASA images and animations of our home planet, available at: *http://visibleearth.nasa.gov/view.php?id=76699*, accessed: 28 November 2012

Papathanassiou, K. P., Mette, T., Hajnsek, I. and Moreira, A. (2005): Polarimetric SAR Interferometry: Potential and Limitations for Biomass Estimation. German Aerospace Center (DLR). Microwaves and Radar Institute (DLR-HR), available at: *http://www.eorc.jaxa.jp/ALOS/kyoto/feb2005/pdf/9-KC6_Papathanassiou.pdf*, accessed: 13 November 2012

The Local (2011): Sweden's news in English, available at: *http://www.thelocal.se/36120/20110913/#.UMnWyIPhrls*, accessed: 02 December 2012

Zianis, D., Muukkonen, P., Mäkipää, R. and Mencuccini M. (2005): Biomass and Stem Volume Equations for Tree Species in Europe. The Finnish Society of Forest Science. The Finnish Forest Research Institute, available at: *http://www.metla.fi/silvafennica/full/smf/smf004.pdf*, accessed: 19 September 2012

Appendices

Appendix 1. Summary statistics of forest inventory parameters in measured plots (15m by 15m). The spatial location of these plots can be found in Appendix 2.

#	Dominant species	AGB (kg/plot)	AGB (kg/m^2)	Tree count	#	Dominant species	AGB (kg/plot)	AGB (kg/m^2)	Tree count
1	Spruce	6157.6	27.37	26	**43**	Pine	2325.8	10.34	27
2	Pine	4107.3	18.25	29	**44**	Spruce	7429.0	33.02	18
3	Birch	3436.0	15.27	23	**45**	Mixed	4955.4	22.02	55
4	Spruce	3626.3	16.12	27	**46**	Spruce	4915.8	21.85	20
5	Pine	569.7	2.53	33	**47**	Spruce	4696.8	20.87	18
6	Birch	3610.4	16.05	36	**48**	Pine	3349.8	14.89	27
7	Spruce	6718.3	29.86	57	**49**	Spruce	7448.4	33.10	12
8	Spruce	6355.9	28.25	17	**50**	Spruce	860.7	3.83	39
9	Spruce	1671.3	7.43	68	**51**	Pine	1828.3	8.13	34
10	Pine	2820.4	12.53	6	**52**	Spruce	3639.3	16.17	24
11	Spruce	556.5	2.47	63	**53**	Spruce	4301.3	19.12	9
12	Pine	1926.6	8.56	23	**54**	Spruce	3736.9	16.61	24
13	Spruce	7025.8	31.23	15	**55**	Pine	1232.6	5.48	17
14	Mixed	3509.5	15.60	52	**56**	Pine	987.2	4.39	26
15	Spruce	4714.7	20.95	29	**57**	Pine	1756.4	7.81	33
16	Birch	3028.7	13.46	32	**58**	Pine	850.2	3.78	34
17	Spruce	1195.0	5.31	81	**59**	Pine	2911.9	12.94	34
18	Pine	4049.1	18.00	18	**60**	Spruce	4332.8	19.26	32
19	Pine	2370.6	10.54	19	**61**	Pine	2831.6	12.59	28
20	Spruce	789.2	3.51	60	**62**	Spruce	4748.0	21.10	19
21	Birch	787.4	3.50	90	**63**	Spruce	5621.2	24.98	23
22	Spruce	3829.6	17.02	36	**64**	Mixed	3142.2	13.97	63
23	Spruce	1506.0	6.69	16	**65**	Spruce	3232.9	14.37	68
24	Spruce	5893.5	26.19	17	**66**	Spruce	3457.1	15.36	25
25	Spruce	7566.1	33.63	17	**67**	Pine	1403.5	6.24	93
26	Birch	3803.4	16.90	29	**68**	Spruce	4591.9	20.41	19
27	Pine	1293.7	5.75	70	**69**	Pine	4132.7	18.37	39
28	Spruce	832.0	3.70	61	**70**	Spruce	640.0	2.84	45
29	Pine	1234.5	5.49	23	**71**	Spruce	7515.3	33.40	15
30	Spruce	6276.5	27.90	14	**72**	Birch	2039.0	9.06	50
31	Pine	2657.2	11.81	29	**73**	Mixed	2582.2	11.48	78
32	Pine	1453.9	6.46	19	**74**	Spruce	3520.2	15.65	89
33	Spruce	6718.8	29.86	12	**75**	Spruce	5330.9	23.69	15
34	Spruce	1939.9	8.62	59	**76**	Spruce	4375.1	19.44	23
35	Spruce	6576.5	29.23	16	**77**	Mixed	1296.2	5.76	56
36	Pine	1940.9	8.63	21	**78**	Birch	2258.0	10.04	9
37	Pine	1392.1	6.19	19	**79**	Spruce	3153.1	14.01	27
38	Pine	2707.7	12.03	17	**80**	Spruce	882.0	3.92	49
39	Birch	2789.8	12.40	45	**81**	Spruce	5828.3	25.90	39
40	Pine	2476.2	11.01	19	**82**	Pine	898.9	4.00	138
41	Pine	1147.6	5.10	90	**83**	Spruce	5373.5	23.88	18
42	Spruce	9881.0	43.92	23					

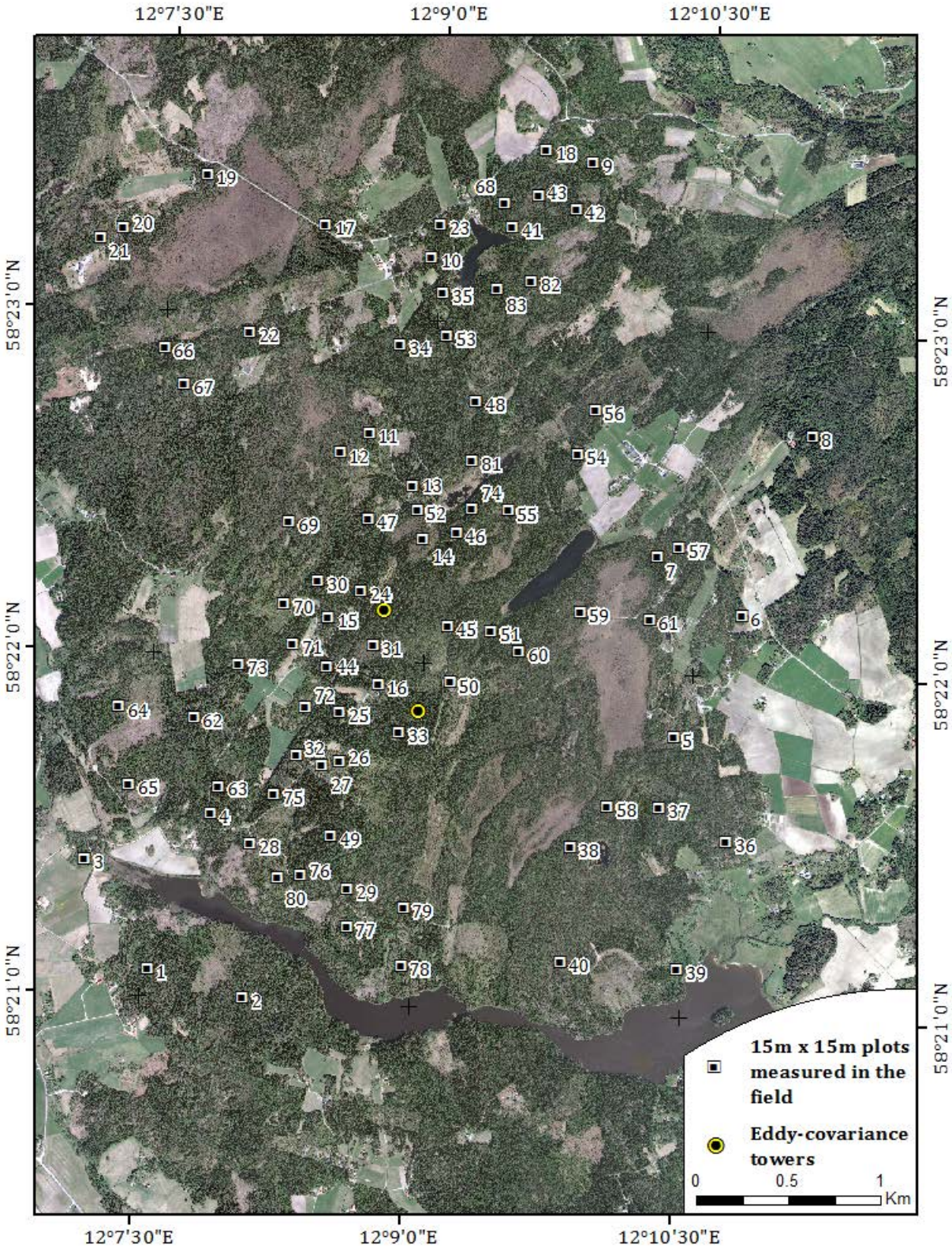

Appendix 2. Orthophoto of the Skogaryd area with location of plots measured in the field (1 m pixel resolution). The orthophoto image was provided by *@ Lantmäteriet, Dnr: i2012/927.*

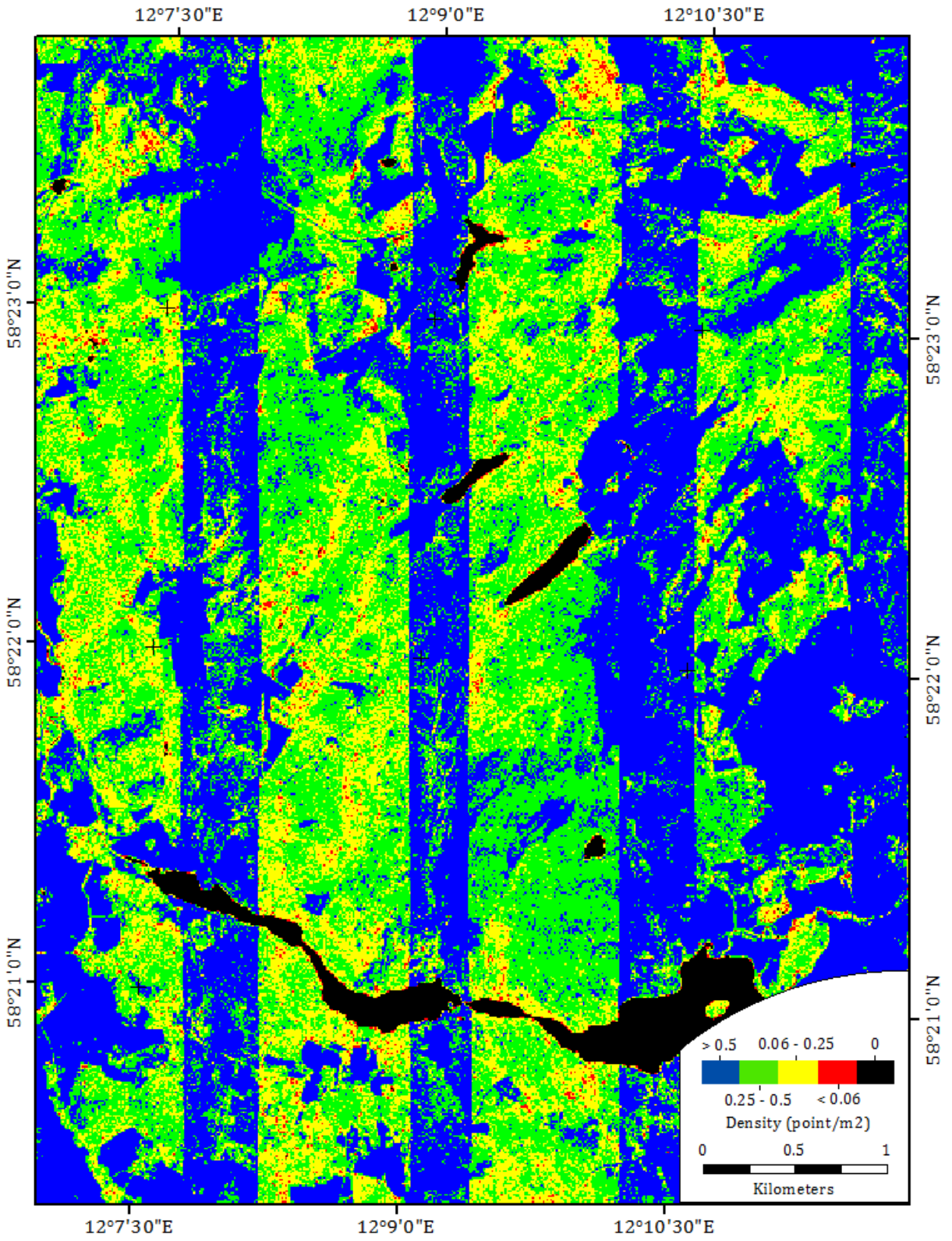

Appendix 3. Density of LiDAR point cloud over the Skogaryd area (10 m pixel resolution). Source: @ *Lantmäteriet, Dnr: i2012/927.*

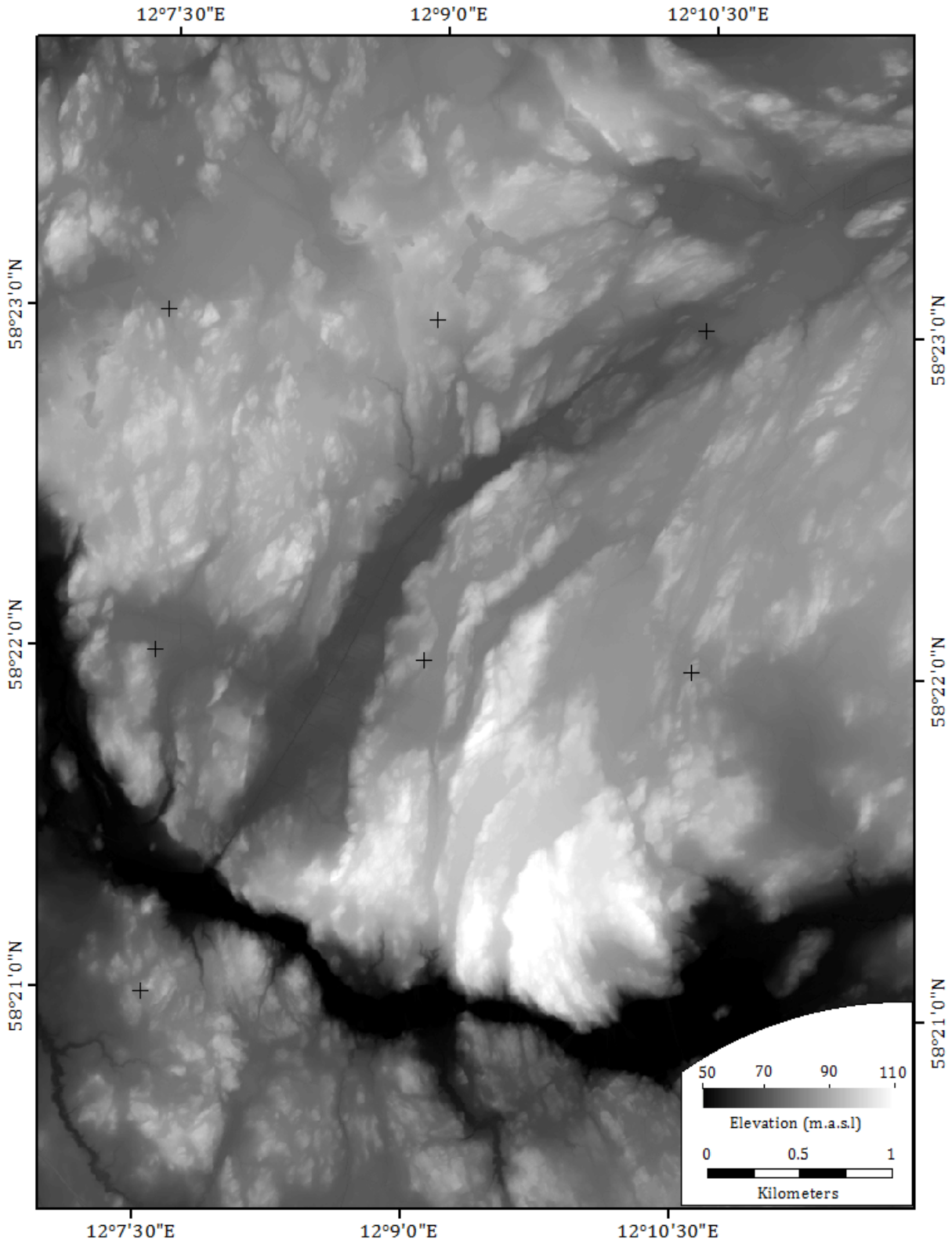

Appendix 4. Digital terrain model (DTM) of the Skogaryd area (3 m pixel resolution).

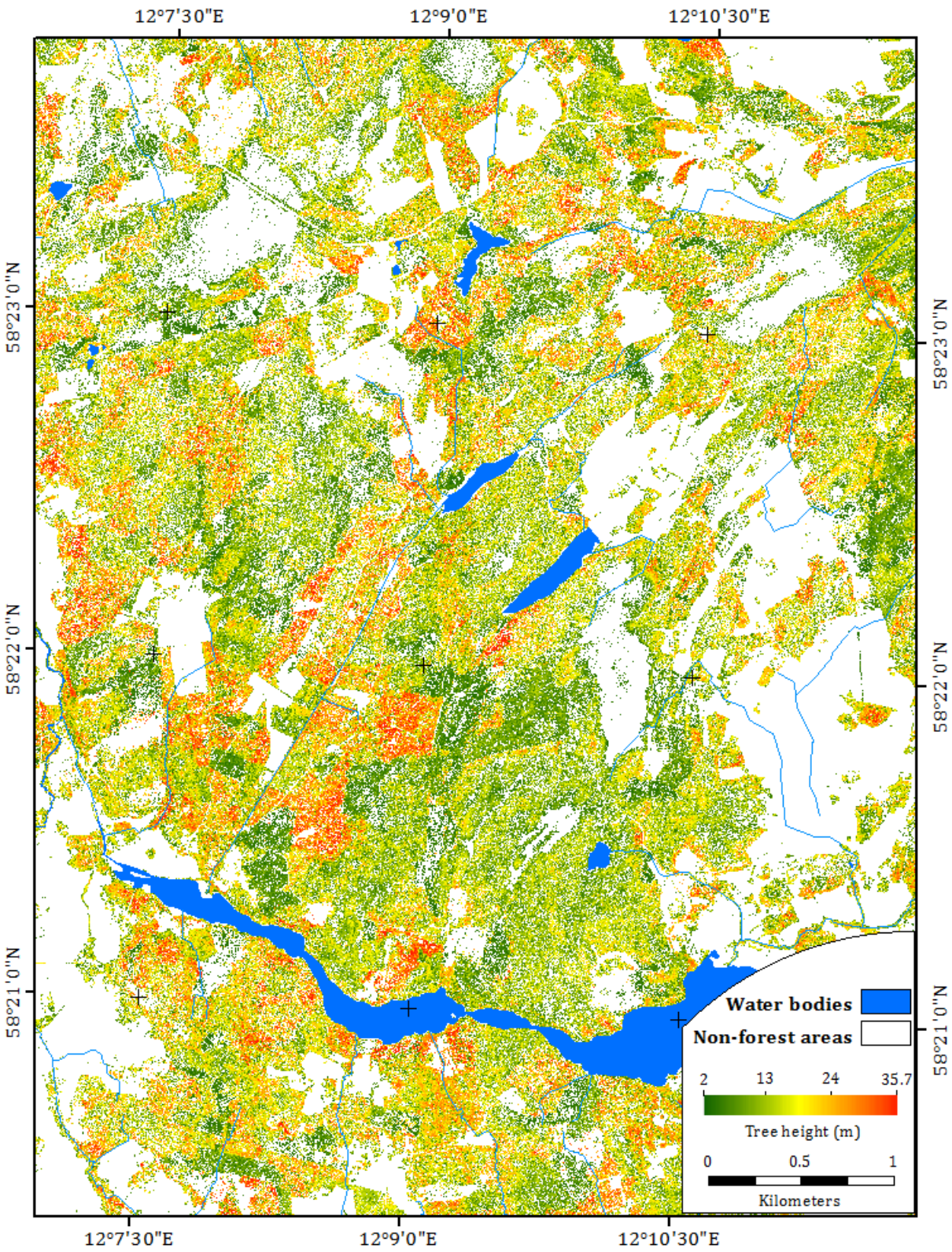

Appendix 5. Canopy height model (CHM) of the Skogaryd area (0.5 m pixel resolution). Water bodies layer was provided by: *@ Lantmäteriet, Dnr: i2012/927.*

Institutionen för naturgeografi och ekosystemvetenskap, Lunds Universitet.

Student examensarbete (Seminarieuppsatser). Uppsatserna finns tillgängliga på institutionens geobibliotek, Sölvegatan 12, 223 62 LUND. Serien startade 1985. Hela listan och själva uppsatserna är även tillgängliga på LUP student papers (www.nateko.lu.se/masterthesis) och via Geobiblioteket (www.geobib.lu.se)

The student thesis reports are available at the Geo-Library, Department of Physical Geography and Ecosystem Science, University of Lund, Sölvegatan 12, S-223 62 Lund, Sweden. Report series started 1985. The complete list and electronic versions are also electronic available at the LUP student papers (www.nateko.lu.se/masterthesis) and through the Geo-library (www.geobib.lu.se)

200 Naemi Gunlycke & Anja Tuomaala (2011): Detecting forest degradation in Marakwet district, Kenya, using remote sensing and GIS

201 Nzung Seraphine Ebang (2011): How was the carbon balance of Europe affected by the summer 2003 heat wave? A study based on the use of a Dynamic Global Vegetation Model; LPJ-GUESS

202 Per-Ola Olsson (2011): Cartography in Internet-based view services – methods to improve cartography when geographic data from several sources are combined

203 Kristoffer Mattisson (2011): Modelling noise exposure from roads – a case study in Burlövs municipality

204 Erik Ahlberg (2011): BVOC emissions from a subarctic Mountain birch: Analysis of short-term chamber measurements.

205 Wilbert Timiza (2011): Climate variability and satellite – observed vegetation responses in Tanzania.

206 Louise Svensson (2011): The ethanol industry - impact on land use and biodiversity. A case study of São Paulo State in Brazil.

207 Fredrik Fredén (2011): Impacts of dams on lowland agriculture in the Mekong river catchment.

208 Johanna Hjärpe (2011): Kartläggning av kväve i vatten i LKAB:s verksamhet i Malmberget år 2011 och kvävets betydelse i akvatiska ekosystem ur ett lokalt och ett globalt perspektiv

209 Oskar Löfgren (2011): Increase of tree abundance between 1960 and 2009 in the treeline of Luongastunturi in the northern Swedish Scandes

210 Izabella Rosengren (2011): Land degradation in the Ovitoto region of Namibia: what are the local causes and consequences and how do we avoid them?

211 Irina Popova (2011): Agroforestry och dess påverkan på den biofysiska miljön i Afrika.

212 Emilie Walsund (2011): Food Security and Food Sufficiency in Ethiopia and Eastern Africa.

213 Martin Bernhardson (2011): Jökulhlaups: Their Associated Landforms and Landscape Impacts.

214 Michel Tholin (2011): Weather induced variations in raptor migration; A study of raptor migration during one autumn season in Kazbegi, Georgia, 2010

215 Amelie Lindgren (2011) The Effect of Natural Disturbances on the Carbon Balance of Boreal Forests.

216 Klara Århem (2011): Environmental consequences of the palm oil industry in Malaysia.

217 Ana Maria Yáñez Serrano (2011) Within-Canopy Sesquiterpene Ozonolysis in Amazonia
218 Edward Kashava Kuliwoye (2011) Flood Hazard Assessment by means of Remote Sensing and Spatial analyses in the Cuvelai Basin Case Study Ohangwena Region –Northern Namibia
219 Julia Olsson (2011) GIS-baserad metod för etablering av centraliserade biogasanläggningar baserad på husdjursgödsel.
220 Florian Sallaba (2011) The potential of support vector machine classification of land use and land cover using seasonality from MODIS satellite data
221 Salem Beyene Ghezahai (2011) Assessing vegetation changes for parts of the Sudan and Chad during 2000-2010 using time series analysis of MODIS-NDVI
222 Bahzad Khaled (2011) Spatial heterogeneity of soil CO2 efflux at ADVEX site Norunda in Sweden
223 Emmy Axelsson (2011) Spatiotemporal variation of carbon stocks and fluxes at a clear-cut area in central Sweden
224 Eduard Mikayelyan (2011) Developing Android Mobile Map Application with Standard Navigation Tools for Pedestrians
225 Johanna Engström (2011) The effect of Northern Hemisphere teleconnections on the hydropower production in southern Sweden
226 Kosemani Bosede Adenike (2011) Deforestation and carbon stocks in Africa
227 Ouattara Adama (2011) Mauritania and Senegal coastal area urbanization, ground water flood risk in Nouakchott and land use/land cover change in Mbour area
228 Andrea Johansson (2011) Fire in Boreal forests
229 Arna Björk Þorsteinsdóttir (2011) Mapping *Lupinus nootkatensis* in Iceland using SPOT 5 images
230 Cléber Domingos Arruda (2011) Developing a Pedestrian Route Network Service (PRNS)
231 Nitin Chaudhary (2011) Evaluation of RCA & RCA GUESS and estimation of vegetation-climate feedbacks over India for present climate
232 Bjarne Munk Lyshede (2012) Diurnal variations in methane flux in a low-arctic fen in Southwest Greenland
233 Zhendong Wu (2012) Dissolved methane dynamics in a subarctic peatland
234 Lars Johansson (2012) Modelling near ground wind speed in urban environments using high-resolution digital surface models and statistical methods
235 Sanna Dufbäck (2012) Lokal dagvattenhantering med grönytefaktorn
236 Arash Amiri (2012)Automatic Geospatial Web Service Composition for Developing a Routing System
237 Emma Li Johansson (2012) The Melting Himalayas: Examples of Water Harvesting Techniques
238 Adelina Osmani (2012) Forests as carbon sinks - A comparison between the boreal forest and the tropical forest
239 Uta Klönne (2012) Drought in the Sahel – global and local driving forces and their impact on vegetation in the 20th and 21st century
240 Max van Meeningen (2012) Metanutsläpp från det smältande Arktis
241 Joakim Lindberg (2012) Analys av tillväxt för enskilda träd efter gallring i ett blandbestånd av gran och tall, Sverige
242 Caroline Jonsson (2012) The relationship between climate change and grazing

by herbivores; their impact on the carbon cycle in Arctic environments

243 Carolina Emanuelsson and Elna Rasmusson (2012) The effects of soil erosion on nutrient content in smallholding tea lands in Matara district, Sri Lanka

244 John Bengtsson and Eric Torkelsson (2012) The Potential Impact of Changing Vegetation on Thawing Permafrost: Effects of manipulated vegetation on summer ground temperatures and soil moisture in Abisko, Sweden

245 Linnea Jonsson (2012). Impacts of climate change on Pedunculate oak and Phytophthora activity in north and central Europe

246 Ulrika Belsing (2012) Arktis och Antarktis föränderliga havsistäcken

247 Anna Lindstein (2012) Riskområden för erosion och näringsläckage i Segeåns avrinningsområde

248 Bodil Englund (2012) Klimatanpassningsarbete kring stigande havsnivåer i Kalmar läns kustkommuner

249 Alexandra Dicander (2012) GIS-baserad översvämningskartering i Segeåns avrinningsområde

250 Johannes Jonsson (2012) Defining phenology events with digital repeat photography

251 Joel Lilljebjörn (2012) Flygbildsbaserad skyddszonsinventering vid Segeå

252 Camilla Persson (2012) Beräkning av glaciärers massbalans – En metodanalys med fjärranalys och jämviktslinjehöjd över Storglaciären

253 Rebecka Nilsson (2012) Torkan i Australien 2002-2010 Analys av möjliga orsaker och effekter

254 Ning Zhang (2012) Automated plane detection and extraction from airborne laser scanning data of dense urban areas

255 Bawar Tahir (2012) Comparison of the water balance of two forest stands using the BROOK90 model

256 Shubhangi Lamba (2012) Estimating contemporary methane emissions from tropical wetlands using multiple modelling approaches

257 Mohammed S. Alwesabi (2012) MODIS NDVI satellite data for assessing drought in Somalia during the period 2000-2011

258 Christine Walsh (2012) Aerosol light absorption measurement techniques: A comparison of methods from field data and laboratory experimentation

259 Jole Forsmoo (2012) Desertification in China, causes and preventive actions in modern time

260 Min Wang (2012) Seasonal and inter-annual variability of soil respiration at Skyttorp, a Swedish boreal forest

261 Erica Perming (2012) Nitrogen Footprint vs. Life Cycle Impact Assessment methods – A comparison of the methods in a case study.

262 Sarah Loudin (2012) The response of European forests to the change in summer temperatures: a comparison between normal and warm years, from 1996 to 2006

263 Peng Wang (2012) Web-based public participation GIS application – a case study on flood emergency management

264 Minyi Pan (2012) Uncertainty and Sensitivity Analysis in Soil Strata Model Generation for Ground Settlement Risk Evaluation

265 Mohamed Ahmed (2012) Significance of soil moisture on vegetation greenness in the African Sahel from 1982 to 2008

266 Iurii Shendryk (2013) Integration of LiDAR data and satellite imagery for biomass estimation in conifer-dominated forest